LC Passive Wireless Sensors Toward a Wireless Sensing Platform: Status, Prospects, and Challenges

Qing-An Huang, *Fellow, IEEE*, Lei Dong, and Li-Feng Wang, *Member, IEEE*

***Abstract*— Inductor–capacitor (*LC*) passive wireless sensors use a transformer with loose coupling between an external readout coil and an inductor that receives power through this inductive coupling. Changes in the sensor are wirelessly and remotely detected by the readout coil, which makes them highly useful in applications that require the sensor to be powered remotely and to occupy a small volume, such as harsh and sealed environments, where physical access to the sensor is difficult. Although the sensor to accomplish this function dates from the 1960's, its rapid extension over the past decades has benefited from microelectromechanical systems. This paper provides an overview of the status and challenges in the *LC* passive wireless sensor toward a wireless sensing platform. The basic sensing principles are first categorized into detecting changes of the sensor in response to the capacitance, resistance, inductance, or coupling distance due to the parameter of interest through monitoring the impedance magnitude and phase spectrum. The present state of the art in sensor applications for pressure, strain, temperature, humidity, biochemical, gas, and so on is then reviewed and compared. For emerging applications from many Internet of Things scenarios, geometrical constraints, such as small and non-invasive coils, reduce the magnetic coupling between the sensor and the readout coil, resulting in a limited interrogation distance. Furthermore, an increasing number of applications also require the simultaneous measurement of multiple parameters. Recent efforts to increase the interrogation distance and to extend the measurement of single parameter to multiple parameters are finally outlined. [2016-0093]**

***Index Terms*— Inductor-capacitor (LC), magnetic coupling, passive, wireless, sensor.**

I. Introduction

INDUCTOR-CAPACITOR (*LC*) passive wireless sensors were proposed by Collins as early as in 1967 [1], which utilized a pair of flat spiral coils to realize a miniature pressure sensor implanting in the eye. However, they have not drawn much attention until to the 1990's [2], [3] with the development of micro-electro-mechanical-system (MEMS) technology.

Manuscript received May 4, 2016; revised August 18, 2016; accepted August 21, 2016. Date of publication September 1, 2016; date of current version September 29, 2016. This work was supported in part by the National Natural Science Foundation of China under Grant 61136006 and Grant 61401084 and in part by the National High Technology Development Program of China under Grant 2015AA042602. Subject Editor G. Stemme.

The authors are with the Key Laboratory of MEMS of the Ministry of Education, Southeast University, Nanjing 210096, China (e-mail: hqa@seu.edu.cn).

Color versions of one or more of the figures in this paper are available online at http://ieeexplore.ieee.org.

Digital Object Identifier 10.1109/JMEMS.2016.2602298

Remote query capability is one of the main advantages of the *LC* sensors. Sensor information can be obtained without physical connections or rigid alignment criteria, thus the *LC* sensors can be applied in situations where wired connection is difficult or even impossible. Examples of these applications are the sensors on moving or rotating parts [4], [5], medical sensing inside human body [6], and sensing under harsh environmental conditions [7]. The other advantage of the *LC* sensors is that they do not require a power source for their operation. This "battery-free" brings two advantages: small size and long lifetime, which makes the *LC* sensors superior in some certain circumstance such as sealed environment [8], biomedical implants [9], etc. The simple structure of the *LC* sensors also achieves low cost. The rapid development of Internet of Things (IoT) [10] for applications such as implantable sensors and wearable devices [11] makes the *LC* passive wireless sensor a hot research field.

This paper provides an overview of the status and challenges of the *LC* passive wireless sensor. Its basic operation principle is first introduced in Section II, including the construction, basic components, sensing principle and portable interrogator. The state of the art applications of the sensor for pressure, strain, temperature, humidity, biochemical, and gas, etc., is then reviewed and compared systematically in Section III. In order to increase the interrogation distance and to develop the sensor from single parameter measurement to multiple parameters, recent efforts have been made. Different approaches to increase the interrogation distance by enhancing the coupling between the external readout coil and the inductor, improving the sensitivity and Q factor of the sensor as well as the signal extraction method, and in particular, adopting a resonant repeater between the external readout coil and the inductor are outlined in Section IV. An attempt to develop the sensor into multi-functions through monitoring both resonant frequency and Q factor, designing a specific winding inductor, and integrating with an on-chip passive switch is also examined in Section IV. Conclusions are finally given in Section V.

II. Operation Principle

An *LC* sensor is typically constructed from a spiral inductor connected with a sensing capacitor, forming a resonant *LC* tank. The capacitor changes in response to the parameter of interest, resulting in a shift in its resonant frequency.

1057-7157 © 2016 IEEE. Translations and content mining are permitted for academic research only. Personal use is also permitted, but republication/redistribution requires IEEE permission. See http://www.ieee.org/publications_standards/publications/rights/index.html for more information.

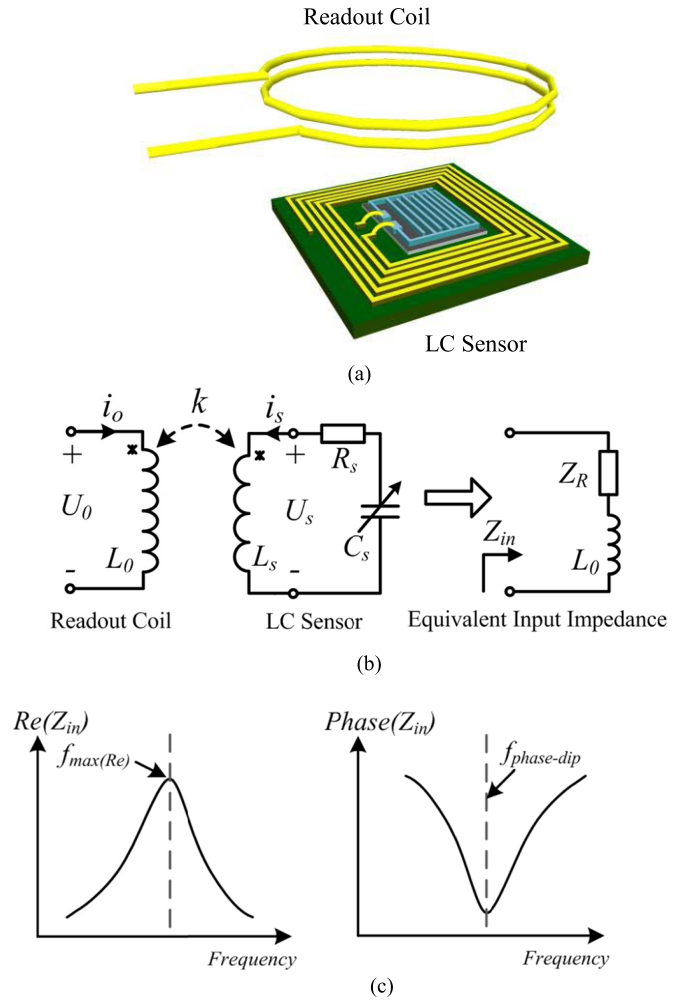

Fig. 1. Schematic representation of an *LC* sensor interrogating system. (a) Schematic representation of an *LC* sensor interrogating system. (b) Equivalent circuit of an *LC* sensor interrogating system. (c) Characteristic curve of $Re\,(Z_{in})$ and $Phase\,(Z_{in})$.

To wirelessly interrogate the *LC* sensor, a readout coil is magnetically coupled with the sensor, and the resonant frequency of the sensor is detected through monitoring the impedance or input return loss of the readout coil. A schematic representation of the typical *LC* sensor is exhibited in Fig.1 (a), and the corresponding equivalent circuit is shown in Fig.1 (b).

A. Construction of an LC Passive Wireless Sensor

According to Kirchhoff's law, an analytical model for the inductive circuit can be represented as [12]

$$U_0 = j\omega L_0 i_0 + j\omega M i_s \tag{1}$$

$$U_s = j\omega L_s i_s + j\omega M i_0 = -R_s i_s - \frac{i_s}{j\omega C_s} \tag{2}$$

where U_0, U_s, i_0, and i_s are defined as shown in Fig.1 (b). The mutual inductance M of the coupled coils can be written as

$$M = k\sqrt{L_0 L_s} \tag{3}$$

where k is the geometry-dependent coupling coefficient with a value between 0 (no coupling) and ± 1 (maximum coupling).

The equivalent input impedance Z_{in} at the terminals of the readout coil is derived using Eqs.(1) and (2) as

$$Z_{in} = \frac{U_0}{i_0} = j\omega L_0 + Z_R = j\omega L_0 + \frac{\omega^2 M^2}{R_s + j\omega L_s + 1/j\omega C_s}. \tag{4}$$

Using the following substitutions,

$$f_s = \frac{1}{2\pi\sqrt{L_s C_s}}, \tag{5}$$

$$Q = \frac{1}{R_s}\sqrt{\frac{L_s}{C_s}}, \tag{6}$$

where Q is the quality factor of the *LC* sensor, and f_s is the resonant frequency of the sensor, then the real part, the imaginary part, and the real part maximum of Z_{in} can be written as

$$Re\,(Z_{in}) = 2\pi f L_0 k^2 Q \frac{\frac{f}{f_s}}{1 + Q^2(\frac{f}{f_s} - \frac{f_s}{f})^2}, \tag{7}$$

$$Im\,(Z_{in}) = 2\pi f L_0 [1 + k^2 Q^2 \frac{1 - (\frac{f}{f_s})^2}{1 + Q^2(\frac{f}{f_s} - \frac{f_s}{f})^2}], \tag{8}$$

$$Z_{max} = Re\,(Z_{in})_{max}\,|_{f=f_s} = 2\pi f_s L_0 k^2 Q. \tag{9}$$

In practical detection, the input impedance will undergo a phase rotation when one moves along the line from the terminals of the readout coil to the port of the measurement equipment due to the transmission line effect at higher frequency. Actually, it has little effect on the input impedance detected when the testing frequency domain is of tens megahertz. The Q factor detected at the measurement device is not the unloaded Q factor in Eq.(6) but a loaded Q factor as

$$Q_L = \frac{Q}{1 + \kappa}, \tag{10}$$

which is dependent of a coupling factor κ of the transmission line [13].

The resonant frequency f_s can be obtained from the maximum of $Re(Z_{in})$ as shown in Fig. 1 (c),

$$f_{\max(Re)} = \sqrt{\frac{2Q^2}{2Q^2 - 1}} \times f_s \approx (1 + \frac{1}{4Q^2}) f_s. \tag{11}$$

It is noticing that $f_{max(Re)}$ is only related with f_s and Q which are intrinsic parameters of the *LC* sensor. In normal circumstance, i.e., $\frac{1}{4Q^2} \ll 1$, $f_{\max(Re)}$ is approximately considered as f_s.

The phase $\angle Z_{in}$ can be expressed as

$$\angle Z_{in} = arctan \frac{Im\,(Z_{in})}{Re\,(Z_{in})}. \tag{12}$$

By solving the equation:

$$\frac{\partial \angle Z_{in}}{\partial f} = 0. \tag{13}$$

The frequency at which the impedance phase minimum occurs is derived as

$$f_{phase-dip} \approx (1 + \frac{1}{4}k^2 + \frac{1}{8Q^2}) f_s. \tag{14}$$

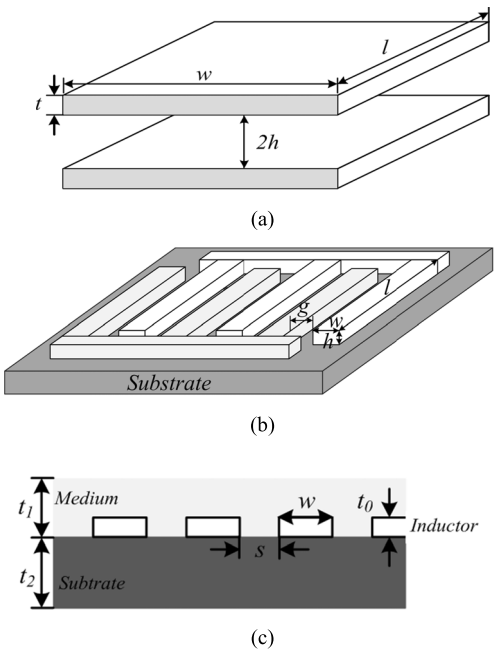

Fig. 2. Representation of capacitor models. (a) Parallel-plate capacitor model. (b) Interdigital capacitor model. (c) Parasitic capacitor model in a spiral planar inductor.

It is observed that $f_{phase-dip}$ is not only dependent of the intrinsic parameters f_s and Q, but also the coupling coefficient k, which is affected by the location of the readout coil and the sensor inductor. Hence there are two points to note when the phase dip measurement is used [12]: one is to fix positions of the readout coil and the sensor inductor to ensure a constant k, and the other is to keep $\frac{1}{4}k^2 \ll 1$ to ensure that $f_{phase-dip} \approx f_s$.

B. Basic Components

An *LC* sensor is constructed using only three basic components: capacitor, inductor, and resistor, and each of them can respond to the parameter of interest to shift the resonant frequency and alter the Q-factor of the sensor.

1) Capacitor: The structure of a sensitive capacitor usually falls into two categories: parallel plate and interdigital. Sometimes, however, a parasitic capacitor is regarded as a sensitive one in literatures for absence of the external capacitor connected to the inductor, which makes the inductor self as an *LC* sensor element. Besides, the varactor diode is also considered as a kind of sensitive capacitor when biotelemetric systems are used. Modeling of these capacitors has been well established, which is briefly introduced as follows.

For a parallel plate capacitor with dimensions as shown in Fig.2 (a), the capacitance per unit length taking the fringe effect into account can be written as [14]

$$C_p = \varepsilon \frac{w}{h}[1 + \frac{h}{\pi w} + \frac{h}{\pi w}\ln\left(\frac{2\pi w}{h}\right) + \frac{h}{\pi w} ln(1 + \frac{2t}{h} + 2\sqrt{\frac{t}{h} + \frac{t^2}{h^2}})] \quad (15)$$

where ε is the dielectric constant. The right side of Eq.(15) includes four items: the first term defines the capacitance of the simple parallel-plate capacitor, the second and third terms are the fringing field due to the finite dimensions of the plates, and the fourth term is the fringing field associated with the thickness of the plates. It should be noted that the fringing effect in this equation is limited to two-dimension due to the conformal mapping, hence the model is accurate when $l > w$ as the fringing along l axis at the corners is omitted.

For most applications using sensitive parallel-plate capacitor, the simplified formula for calculating the capacitance is

$$C = A\frac{\varepsilon_0 \varepsilon_r}{D} \quad (16)$$

where A is the area of the plate, D is the distance between the two electrodes, ε_r is the relative dielectric, and $\varepsilon_0 = 8.85 \times 10^{-12}$ F/m.

For an interdigital capacitor in air environment as shown in Fig.2 (b), the total capacitance is written as [15]

$$C = (N-1)\,\varepsilon l[\frac{K(\xi')}{K(\xi)} + \frac{h}{g}] \quad (17)$$

where N is the number of its finger pares, $K(\xi)$ is the complete elliptic integral of the first kind, and ξ and ξ' are defined as

$$\xi = \sin(\frac{\pi}{2}\frac{g}{w+g}) \quad (18)$$

$$\xi' = \sqrt{1-\xi^2}. \quad (19)$$

The capacitance calculation formula in Eq.(17) can also be simplified into the form like Eq. (16) by removing the first term in the bracket.

For the parasitic capacitor in a planar spiral inductor as shown in Fig. 2 (c), the capacitance per unit length is [16]

$$C_{ext} = \varepsilon_{r-eff} C_0 \quad (20)$$

where C_0 is the capacitance between adjacent traces in free space, and it can be expressed as

$$C_0 = \varepsilon_0 \frac{K(\xi_0')}{K(\xi_0)} \quad (21)$$

where $K(\xi_0)$ is the complete elliptic integral of the first kind, and $\xi_0 = 2s/(s+2w)$, and $\xi_0' = (1-\xi_0^2)^{1/2}$. The ε_{r-eff} in Eq. (20) is the equivalent relative dielectric, and can be written as

$$\varepsilon_{r-eff} = 1 + \frac{1}{2}(\varepsilon_{r1}-1)\frac{K(\xi_0)\,K(\xi_1')}{K(\xi_0')K(\xi_1)} + \frac{1}{2}(\varepsilon_{r2}-1)\frac{K(\xi_0)\,K(\xi_2')}{K(\xi_0')K(\xi_2)} \quad (22)$$

with

$$\xi_i = \frac{\tanh(\frac{\pi s}{4t_i})}{\tanh(\frac{\pi(s+2w)}{4t_i})}, \quad (23)$$

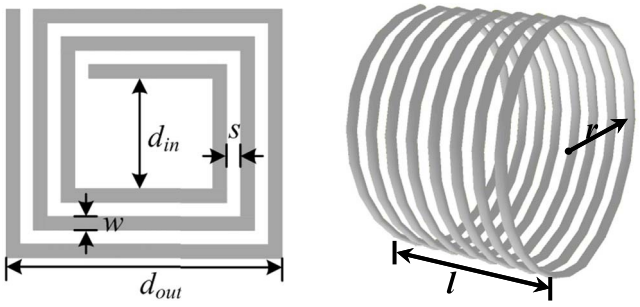

Fig. 3. Planar spiral inductor and solenoidal inductor.

where $\xi_i' = (1-\xi_i^2)^{1/2}$, ε_{ri} is the relative dielectric of the medium and substrate, and t_i is the corresponding thickness. Similar to Eq.(15), the conformal mapping is also used in Eq.(17) and Eq.(22). Hence, the condition $l > w$ should be satisfied to make the model accurate.

A varactor diode is another kind of sensitive capacitor. It is usually described by the small signal junction capacitance of the voltage dependent capacitor in the sensing circuit. In the reverse bias state, it is approximated by

$$C(V_C) = \frac{C_A}{\left(1-\frac{V_C}{\varphi}\right)^{1/2}} \tag{24}$$

where C_A is the junction capacitance at zero bias, ϕ is the junction built in potential and V_C is the bias voltage applied across the varactor.

2) Inductor: The most widely used inductors are the planar spiral inductor and solenoidal inductor. Modeling of these capacitors has been well established, which is briefly introduced as follows.

For the planar spiral inductor, a modified wheel formula is the classic loop inductance method [17], which gives the inductance for the planar inductor in Fig.3

$$L = K_1 \mu \frac{N^2 d_{avg}}{1+K_2\rho} \tag{25}$$

where N is the number of turns, and $d_{avg} = (d_{in}+d_{out})/2$ is the average diameter, $\rho = (d_{in}-d_{out})/(d_{in}+d_{out})$ is the fill ratio, μ is the permeability, and K_1 and K_2 are layout dependent which are 2.34 and 2.75, respectively, for the rectangular inductor. This equation can be applied to square, hexagonal, octagonal, and circular inductors.

For the solenoidal inductor, the inductance can be calculated as [18]

$$L = \eta \frac{\mu N^2 \pi r^2}{l} \tag{26}$$

where N is the number of turns, r is the radius of the solenoidal, l is the solenoidal length, and the dimensionless factor η is a function of the ratio l/r.

3) Resistor: A resistor in *LC* sensors refers to the parasitic series resistance of the spiral inductor. It can be calculated as [19], taking the skin effect and proximity effect into account,

$$R_s = R_0\left[1+\frac{t}{\delta\left(1-\exp\left(-\frac{t}{\delta}\right)\right)\left(1+\frac{t}{w}\right)}+\frac{1}{10}\left(\frac{\omega}{\omega_{crit}}\right)^2\right] \tag{27}$$

$$R_0 = \rho_r \frac{l_{sum}}{w\cdot t} \tag{28}$$

$$\omega_{crit} = \frac{3.1\rho_r(w+s)}{\mu w^2 t} \tag{29}$$

where ρ_r is the resistivity of metal, δ is the skin depth, l_{sum} is the total length of the conductor, w is the line width, s is the separation between lines, and t is the thickness of conductor.

C. Sensing Principle

The basic sensing principles are to detect changes of the sensor in response to the capacitance, resistance, inductance or even coupling distance through the physical parameter of interest by monitoring the resonant frequency, input impedance, or Q-factor. By using the total differentiation method, the variations of these qualities due to the parameters of interest can be represented as

$$\begin{aligned}\Delta f_s &= -\frac{1}{4\pi\,(L_sC_s)^{\frac{3}{2}}}(C_s\cdot\Delta L_s + L_s\cdot\Delta C_s)\\ &= -\frac{1}{4\pi\,(L_sC_s)^{3/2}}[C_s\ L_s\ 0]\begin{bmatrix}\Delta L_s\\ \Delta C_s\\ \Delta R_s\end{bmatrix},\end{aligned} \tag{30}$$

$$\begin{aligned}\Delta Q &= \frac{1}{2R_sC_s}\sqrt{\frac{C_s}{L_s}}\cdot\Delta L_s - \frac{L_s}{2R_sC_s^2}\sqrt{\frac{C_s}{L_s}}\\ &\quad\cdot\Delta C_s - \frac{1}{R_s^2}\sqrt{\frac{L_s}{C_s}}\cdot\Delta R_s\\ &= \left[\frac{1}{2R_sC_s}\sqrt{\frac{C_s}{L_s}}\ -\frac{L_s}{2R_sC_s^2}\sqrt{\frac{C_s}{L_s}}\ -\frac{1}{R_s^2}\sqrt{\frac{L_s}{C_s}}\right]\begin{bmatrix}\Delta L_s\\ \Delta C_s\\ \Delta R_s\end{bmatrix},\end{aligned} \tag{31}$$

$$\begin{aligned}\Delta Z_{max} &= 2\pi L_0k^2Q\cdot\Delta f_s + 2\pi L_0f_sk^2\cdot\Delta Q\\ &\quad + 4\pi L_0f_skQ\cdot\Delta k\\ &= \left[2\pi L_0k^2Q\ 2\pi L_0f_sk^2\ 4\pi L_0f_skQ\right]\begin{bmatrix}\Delta f_s\\ \Delta Q\\ \Delta k\end{bmatrix}.\end{aligned} \tag{32}$$

It is noticed that the Q factor of LC sensors is much smaller than other resonators such as piezoelectric crystals. According to Eq. (31), the loss is mainly attributed to the resistance of the metal, complex dielectric permittivity of the capacitor, and magnetic losses caused by the inductor core. The appropriate selection of metal materials with good conductivity is the most effective method to reduce the resistance. Improving the dielectric permittivity of the capacitor is relatively difficult because it depends upon the progress of new sensing principles and materials. Another capacitive element is the parasitic substrate capacitance which is hard to eliminate due to the passive

way (the problem can be solved by the ground connection in an active way). One of the solutions is to fabricate 3D helical inductors in place of planar spiral ones.

To obtain a distinct variation in measurements of the *LC* sensors, the crucial elements are the capacitor C, inductance L, resistor R, and coupling coefficient k. By using the total differentiation method, the concrete analysis of these elements is examined as follows.

1) Capacitive Sensing: Eq.(16) for a capacitor is approximately represented for most of the sensitive capacitors in literatures including the parallel and interdigital capacitors. The capacitance variations can be derived as

$$\Delta C = \frac{\varepsilon_0 \varepsilon_r}{D} \cdot \Delta A + A\frac{\varepsilon_0}{D} \cdot \Delta \varepsilon_r - A\frac{\varepsilon_0 \varepsilon_r}{D^2} \cdot \Delta D. \quad (33)$$

Both the relative dielectric ε_r and area A can cause a linear variation in capacitance, while the distance D does a nonlinear variation in capacitance. The capacitive sensing relies on an external physical parameter changing the spacing, the relative dielectric constant between the two plates, or the plate area. In principle, all sensors which are implemented in capacitive sensing can be transplanted into *LC* passive wireless sensors.

The change of the relative dielectric ε_r is due to the sensitive medium between the electrodes, which responds to the parameter of interest. Depositing the sensitive medium on the capacitor structure is the popular method, and the key point for the sensing method is the selection of medium materials. The sensing mechanism is suitable for both parallel capacitor and interdigital capacitor, and has been used for temperature, humidity, pressure, gas, chemical monitoring in *LC* passive wireless sensors [20]–[22].

Altering the area A requires a movable structure, and few literatures have reported this sensing method in the *LC* passive wireless sensors. In [23], an interdigital capacitor with cascade three-stage bent beam structures was used as the sensitive capacitor to monitor ambient temperature.

Changing the distance D is a relatively simple way to achieve capacitance variation, despite it would create a nonlinear problem. For the parallel plate capacitor, it relies on the force being exerted on the plate electrode to make a deformation, hence most of this kind capacitor are particularly suitable for pressure/force monitoring [24], [25]. For the interdigital capacitor, however, it needs movable structure to complete the sensing mechanism. Structures on flexible substrates respond to external force so as to change the gap between the electrodes [26].

Also, changing relative dielectric ε_r is the effective way to make a parasitic capacitor work as a sensitive element, as expressed in Eq. (20). The capacitor introduced here is first claimed as the parasitic capacitor of the inductor model which is theoretically unwanted in an inductor design. However, this parasitic capacitor can also work as a sensitive part by proper designs. The potential applications focus on the self-resonance of an inductor, for example, the humidity sensing [27].

A varactor is another kind of capacitor, which is the voltage-controlled capacitor. As shown in Eq.(24), its capacitance grows when reverse bias declines. Several studies have utilized the varactor to monitor pH values in solution [28], [29] by examining a shift in the resonant frequency. The pH electrode was connected to the varactor to provide a biasing voltage. As the biasing voltage varied with the solution pH, the capacitance of the varactor changed, causing a change in the *LC* resonant frequency.

2) Inductive Sensing: Inductors used in *LC* passive wireless sensors are generally divided into two categories: the planar spiral inductor and solenoidal inductor as mentioned above.

For a planar spiral inductor, the inductance variations can be derived by Eq. (25) as

$$\Delta L_{pla} = K_1 \mu_0 \frac{N^2 d_{avg}}{1 + K_2 \rho} \cdot \Delta \mu_r + K_1 \mu_0 \mu_r \frac{N^2}{1 + K_2 \rho} \cdot \Delta d_{avg} - K_1 \mu_0 \mu_r \frac{N^2 K_2 d_{avg}}{(1 + K_2 \rho)^2} \cdot \Delta \rho. \quad (34)$$

In terms of practical applications, the relative permeability μ_r plays an important role in altering the inductance, as the other two factors d_{avg} and fill ratio ρ cannot be changed easily in a controlled way. The μ_r change would produce a linear variation in inductance, and is usually implemented by a magnetic core. Kisic *et al.* [30] utilized a ferrite core to test the force: the elastomer deforms due to the force and ferrite approaches to the coil, causing the inductance to change. Special materials, such as magnetostrictive materials, can be used as the coil component in which permeability changes lead to inductance variation [31].

For a solenoidal inductor, the inductance variations can be derived as

$$\Delta L_{solen} = k \mu_0 \frac{N^2 \pi r^2}{l} \cdot \Delta \mu_r + k \mu_0 \mu_r \frac{2N^2 \pi r}{l} \cdot \Delta r - k \mu_0 \mu_r \frac{N^2 \pi r^2}{l^2} \cdot \Delta l. \quad (35)$$

In the case of the relative permeability μ_r, a magnetic core can be inserted to cause the inductance change. For example, some reports used ferromagnetic microwires as a magnetic core to detect the magnetic field [32], [33]. Dimension parameters can respond to strain. The solenoidal inductor for strain measurement was thus reported [34].

3) Resistive Sensing: The resistance change is reflected in the Q-factor and the maximum input impedance, hence it does not draw as much attention as the capacitor and inductor in normal resonant-frequency dependent measurements. The parasitic resistor of the inductor may be simply expressed as Eq.(27). The resistance variations can be derived as

$$\Delta R_0 = \frac{l_{sum}}{w \cdot t} \cdot \Delta \rho_r + \frac{\rho_r}{w \cdot t} \cdot \Delta l_{sum} - \rho_r \frac{l_{sum}}{w \cdot t^2} \cdot \Delta t - \rho_r \frac{l_{sum}}{w^2 \cdot t} \cdot \Delta w. \quad (36)$$

Changing the resistivity ρ_r is a relatively direct approach when compared to dimension parameters such as length and thickness. A temperature sensitive metal has been used as a conductor to monitor the temperature [35], i.e., the resistivity responds to the ambient temperature, causing the resistance change, and hence the Q-factor/input impedance change. Combined with detecting a shift in resonant frequency due to capacitance or inductance, the resistance sensing mechanism is

usually used as a compensation for temperature in *LC* passive wireless sensors [36].

When the cross-section of a resistor is scaled down to nano size, it will exhibit high surface-to-volume ratios, which is sensitive to the specific moieties adsorbed selectively on the surface. Graphene monolayer is a new kind of resistive materials, which is utilized to monitor tooth enamel by *LC* wireless sensors [37]. An alternative is to connect an external sensitive resistor to the inductor [38]. A humidity sensitive resistor based on chemical sintering of silver nanoparticles was utilized to monitor humidity threshold [39].

4) Coupling Distance Sensing: As shown in Eq.(32), the coupling coefficient k only affects the maximum input impedance. It depends on coil configurations, their spacing and relative location. For simplicity, the expression of the coupling coefficient k between two inductors L_1 and L_2 coaxially aligned is given by [40]

$$k = \frac{1}{[1 + 2^{2/3}(\frac{d_{12}}{\sqrt{r_1 r_2}})^2]^{3/2}}. \tag{37}$$

Applying the total differentiation to Eq. (37), it yields

$$\Delta k = \frac{3}{2\left(1 + \frac{2^{2/3}d_{12}^2}{r_1 r_2}\right)^{5/2}}\left(\frac{2^{2/3}d_{12}^2}{r_1^2 r_2} \cdot \Delta r_1 + \frac{2^{2/3}d_{12}^2}{r_1 r_2^2} \cdot \Delta r_2 - \frac{2 \cdot 2^{2/3} d_{12}}{r_1 r_2} \cdot \Delta d_{12}\right) \tag{38}$$

where d_{12} is the distance between the two inductors, and r_1 and r_2 are the radii of the two inductor coils, respectively. The distance d_{12} is the most important factor when the radii r_1 and r_2 cannot be changed easily in a controlled way. Using the k variation to monitor the displacement in *LC* passive wireless sensors is proposed by detecting the input impedance [41].

D. Portable Interrogator

The key to contactless measurement is the inductive coupling: the inductor in *LC* tank acts as the resonant element and the signal antenna concurrently. An external readout coil approaches the *LC* inductor to magnetically couple with the inductor. The electrical parameters of the readout coil are then analyzed to obtain the resonant frequency in the *LC* circuit. There are two measurement methods for the *LC* sensor resonance: measurement in time domain (transient behavior) and measurement in frequency domain (steady state behavior) [31].

A pulse signal is employed to excite the *LC* tank in time domain measurement, and the response signal feedback is collected and analyzed to obtain the resonant frequency [42]. The schematic diagram of working principle is exhibited in Fig.4. A continuous sine wave signal is first sent from the transmitting coil in the transmit phase, and the *LC* tank is energized at the same time in a forced oscillation which has the same frequency as the excitation sine wave. After turning off the excitation signal in the receive phase, the decaying oscillation of the sensor signal is measured through the detecting coil. It should be pointed out that the transmitting coil and the detecting coil can be implemented as the same coil, which only needs a switch to decouple the two signal paths for excitation and reception. The difficulties in this measurement task are a short sensor decay time, and the small amplitude of the receiving signal. It requires a high resolution for the test circuit system which is hard to realize. Thus, most studies have chosen the measurement in frequency domain.

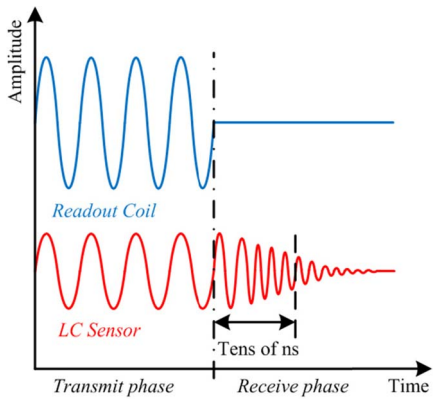

Fig. 4. Measurement in time domain for an *LC* passive wireless sensor.

For measurement in frequency domain, the detection/readout coil and the inductor coil in *LC* tank form a loosely coupled transformer. By using a frequency scan and observing the magnitude and phase information of the readout coil, the sensor reflected impedance can be evaluated and the point of resonance is identified as shown in Fig. 1 (c). In most researches, the input impedance or the S parameter of the inductor is fetched by a commercial impedance/network analyzer which is expensive and has large dimensions. Hence, it is necessary to develop a portable readout device for practical applications.

The signal processer, frequency sweeping module, detection circuit, and the input/output unit are the general cells in most detection systems to achieve automatic sweeping measurement. By using a voltage controlled oscillator (VCO) to excite the *LC* tank, a low power and extremely compact readout circuit realized a mutual distance up to 7.5 mm for a small pressure sensor [6]. The wireless remote sensor platform proposed in [43] can realize an automatic and continuous monitoring of resonant frequency variations in range of 20 kHz ∼10 MHz with a resolution of 0.01 MHz for *in situ* monitoring. Based on a SWR (Standing Wave Ratio) bridge (broadband diode detection), a portable telemetry unit was proposed to implement the extracting resonant frequency within 60 MHz [44]. The input impedance real part was first calculated in the microcontroller, and then plotted in PC post-processing software to find out the peak frequency. A wireless senor interrogator, which was based on frequency modulations spectroscopy (FMS), was proposed not only to enable detection, but also to track the changing resonant frequency of the sensor over time [45]. FMS is a sensitive measurement technique based on changes in amplitude and phase of the frequency components of a frequency modulated (FM) signal. The FM signal is transmitted wirelessly to the *LC* tank, and the *LC* sensor absorbs energy from the transmitted FM signal near its resonant frequency. The *LC* sensor affects both the

TABLE I
PRESSURE SENSORS FOR BIOMEDICAL IMPLANTATION

Reference	Year	C	L	D	Materials	Dimensions	*f* (MHz)	Q	Re(Z_{in}) (Ω)	Resolution	Sensitivity	Range
Collins [1]	1967	--	2.5 μH	--	Glass and mylar	Diameter 2/4/6 mm, Thickness 1/2 mm	168	30	--	0.1 mmHg	--	0~100 mmHg
Rosengren *et al.* [2]	1992	--	--	22 mm	Si	10^2 mm^2	--	5.5	15	--	2 kHz/mmHg	0~200 mmHg
Puers *et al.* [46]	2000	23 pF	0.5 μH	--	Si	5×3×1 mm^3	45	30	1.2	--	--	--
Fonseca *et al.* [47]	2006	--	--	≥20 cm	PTFE/FEP	Diameter: 4 mm	--	65-77	--	--	-1~-20 kHz/mmHg	--
Chen *et al.* [48]	2008	3.1 pF	0.36 μH	2 mm	Parylene	4×1 mm^2	150	5	72	1 mmHg	>7000 ppm/mmHg	--
Chen *et al.* [49]	2010	3.6 pF	57 nH	>2 cm	Parylene C	4×1.5×1 mm^3	~350	~30	4.2	1 mmHg	695 ppm/mmHg	--
Zhai *et al.* [50]	2010	--	7.62 μH	--	Si	6^2×1 mm^3	20	73	11.58	--	40.27 kHz	0~350 mmHg
Luo *et al.* [51]	2012		1.9 μH	3 mm	Zinc and polymer	Diameter: 10 mm	~50	>25	--	--	-290 kHz/kPa	0~30 kPa
Xue *et al.* [52]	2012	0.79 pF	515 nH	6 mm	SU-8 and Au	3.23×1.52×0.2 mm^3	250	21.3	--	<1 mmHg	7035 ppm/mmHg	0-60 mmHg
Chitnis *et al.* [53]	2013	5 pF	1.3 μH	--	Polyimide, stainless steel, Si	Capacitor 2^2×0.8 mm^3 Coil: diameter 5 mm Needle: length 5 mm	63	26.5	14.5	1 mmHg	15 kHz/kPa	0~50 mmHg
Kim *et al.* [54]	2014	0.1 μF	408 nH	7 cm	PDMS, PZT	40×8^{2}π mm^3	0.268	--	--	--	1 kHz/cmH_2O	0~20 cmH_2O
Chen *et al.* [55]	2014	--	--	15 mm	Polyamide and Cu	1^2×0.1 mm^3	2777	--	--	0.3 mmHg	-2.254 MHz/mmHg	0~500 mmHg

Nominal values of the sensors are listed, D denotes the interrogating distance, and k denotes the coupling coefficient.

amplitude and phase of the three frequency components of FM signal, which is used to detect the resonant frequency.

III. STATE OF THE ART

Since the first *LC* passive wireless sensor was proposed in 1967, it has been developed in various fields. In this section, different categories of the sensors are reviewed and compared according to their applications.

A. Pressure Sensor

Pressure monitoring is essential in many fields, including medical, atmosphere, industrial, agriculture, and biochemical, etc.. An *LC* type pressure sensor has superiorities in testing pressure in harsh environment, such as in high temperature applications like turbine engines and compressors, and in sealed environment such as tires, the human body or sealed food. Pressure sensing is one of the most important applications for the *LC* sensors, and is mainly classified here into two categories: pressure sensors for implantation in biomedical monitoring and for industrial and environmental monitoring.

1) Pressure Sensors for Biomedical Implantation: The progress on this area is summarized in Table I. Since the first pressure sensor was applied in the eye [1], more and more researches focus on the implantable sensor for biomedical applications, especially the intraocular pressure (IOP) monitoring. A system for continuous monitoring of IOP consisted of a sensitive capacitor and a gold-wire coil [2]. Puers *et al.* utilized electrodeposited copper inductors to realize IOP monitoring [46]. The dual layer inductor was fabricated by micromachining process to realize the structure. Two types of wireless flexible pressure sensors were introduced in [47]. One was designed for acute use and the other was for chronic use. Various flexible substrates were tested and characterized, including polyimide-acrylic, LCP (Liquid Crystal Polymer)/expanded PTFE (polytetrafluoroethylene), PTFE/FEP (Fluorinated Ethylene Propylene copolymer). Chen *et al.* used Parylene as a biocompatible structure material for minimally invasive intraocular implantation [48]. Instead of having a fixed inductor surrounding the capacitor, a variable inductor can be realized by embedding the top metal wire layer in the diaphragm to alter the intrinsic mutual inductance of the dual-layer inductor. The variable inductor and capacitor achieve high pressure sensitivity. In 2010, they then used a Parylene to create a flexible coil substrate that can be folded to achieve minimally invasive implantation, while stretched back without damage to have a long readout distance [49]. Both of the IOP sensors have been tested through six-month chronic in *vivo* and acute ex *vivo* animal studies. MEMS technology was used to fabricate a miniature pressure sensor for aneurysm sac pressure information [50]. A wireless RF pressure sensor made entirely of biodegradable materials was proposed for short-term, acute medical applications [51]. Metal zinc, which

TABLE II
PRESSURE SENSORS FOR INDUSTRY AND ENVIRONMENTS

Reference	Year	C	L	D	Materials	Dimension	(MHz)	Q	$Re(Z_{in})$ (Ω)	T(K)	Resolution	Sensitivity	Range
Husak *et al.* [56]	1997	19.4 pF	143 μH	--	Si	3^2 mm^2	35.8	3.268	--	--	--	--	--
Park *et al.* [57]	1998	3 pF	220 nH	--	Si and glass	3^2×0.6 mm^3	120	--	3	--	--	2 MHz/mmHg	0~100 mmHg
English *et al.* [58]	1999	--	--	--	Ceramic and Cu	1.5 inch^2	--	--	--	200	--	2.6 MHz/bar	0~100 bar
Akar *et al.* [60]	2001	2 pF	1.2 μH	2 mm	Si and glass	2.6×1.6 mm^2	76	8	--	--	--	1579 ppm/mmHg	0~50 mmHg
DeHennis *et al.* [25]	2002	--	3.7 μH	3 cm	Si	6^2×0.5 mm^3	--	>30	--	--	--	3.2 kHz/mmHg	400~1000 mmHg
Fonseca *et al.* [59]	2002	--	4.2 μH	k= 0.19	Ceramic	3.8^2 cm^2	16.99	61.9	--	400	24 mbar	-141 kHz/bar	0~7 bar
Baldi *et al.* [61]	2003	--	1.7 μH	--	Si and ferrite	3^2 mm^2	31.8	5.4	--	--	--	9.6 kHz/kPa	-40~130 kPa
Shin *et al.* [63]	2005	--	2.14 9mH	--	Polyimide, Cu, Au	--	150.9	--	--	--	--	11.25 kHz/kPa	0~213.3 kPa
Radosavljevic *et al.* [64]	2009	7.69 pF	7.57 μH	--	Ceramic	56.4×40.7 ×0.56 mm^3	20.854	--	17. 48	--	--	25.6 kHz/bar	0-3 bar
Chitnis *et al.* [62]	2013	--	1 μH	6 mm	Polyimide, acrylic, Cu	2×12^2 π mm^3	109	--	--	--	--	3 kHz/kPa	0~60 mmHg

Nominal values of the sensors are listed, D denotes the interrogating distance, and k denotes the coupling coefficient.

is found to be degradable in saline, was used as the sensor conductor material, and biodegradable polymers were used as dielectric and structural materials. A biocompatible SU-8 based intraocular pressure senor, constructed from a planar spiral gold coil and a two-parallel-gold-plate capacitor, was both tested in air and saline [52]. In 2011, a minimally invasive implantable sensor for IOP monitoring was presented [53]. The device consisted of three main components: a hypodermic needle, a micromachined capacitor connected to the needle back-end, and a flexible polyimide coil connected to the capacitor. Most parts of the senor sit externally on the sclera and only the needle penetrated inside the vitreous space, which made the surgery simple while still measuring the true IOP. A mechanical vibration powered implantable pressure sensor was proposed to enhance interrogation range and alleviate the misalignment issue [54]. A piezoelectric cantilever acted as an acoustic receiver and converted sound vibration harmonics into electrical power. The received energy was used to drive the *LC* tank in resonance, thus emitting a series of RF pulses whose frequency was used to indicate the pressure. Chen *et al.* [55] scaled the sensor dimensions down to $1 \times 1 \times 0.1$ cubic millimeters, which would overcome the operating frequency limits of traditional strategies and exhibit insensitivity to lossy tissue environments.

2) Pressure Sensors for Industry and Environments: The progress on this area is summarized in Table II. The CMOS (Complementary Metal Oxide Silicon) process was used to make an integrated pressure sensor by Husak in 1997 [56]. By using bulk micromachining and anodic bonding technologies, a hermetically sealed pressure sensor was then fabricated with a size measured as $3 \times 3 \times 0.6$ mm^3 [57]. Allen *et al.* developed a ceramic pressure sensor with operation temperature up to 200°C, which could be exposed to elevated temperature [58]. They then improved the temperature to 400 °C by using low-temperature co-fired ceramics (LTCC) fabrication technology [59]. In 2001, Akar *et al.* fabricated an absolute pressure sensor by the bulk silicon dissolved wafer process [60]. Based on this process, DeHennis *et al.* proposed a double-sided silicon-on-glass process to integrate an inductor and a capacitive pressure transducer on opposite sides [25]. Ziaie *et al.* has conducted a series of studies on *LC* passive wireless sensors, especially based on the self-resonance of the inductor to cancel the requirement for a separate capacitor [61], [62]. The sensor was based on the ferrite core or magnetic fluid displacement over a planar coil and its corresponding inductance change. Shin *et al.* used chemical etching to fabricate the silicon chips thinner than 50μm for mechanical flexible [63], which overcome the mechanical deformation in elastic region. A fully embedded pressure sensor was also manufactured by a standard LTCC technology for high-temperature and chemical applications [64].

B. Strain Sensor

The progress on this area is summarized in Table III. *LC* strain sensors are desirable for advanced industrial applications, such as point-stress and torque sensing for ball bearings, rotating shafts, and blades. The sensing information is important for optimizing system performance, understanding material fatigue, and achieving reliable system monitoring.

A solenoidal inductor was employed to detect strain [34]: small geometric changes in the solenoid affected its inductance and, as a consequence, the resonant frequency. Strain monitoring of tires in automobiles is very effective for improving the reliability of tires. A strain sensor employed the tires itself was introduced by Matsuzaki and Todoroki [65].

TABLE III
STRAIN SENSORS

Reference	Year	C	L	D	Materials	Dimensions	f (MHz)	Q	Re(Z_{in}) (Ω)	Sensitivity	Range
Butler *et al.* [34]	2002	15 pF	11.4 μH	1.43 cm	--	$0.495\times0.78^2\pi$ cm^3	12.16	--	--	--	0~0.07
Matsuzaki *et al.* [65]	2005	200 pF	10 mH	--	Rubber and steel	--	0.112	--	--	--	0~3000 μ
Jia *et al.* [66]	2006	--	4 μH	120 mm	Polyimide and Cu	~8^2 mm^2	15	--	6.3	--	0~0.018
Saucer *et al.* [31]	2012	83.7 pF	0.29 μH	3 cm	$Fe_{83}Ga_{17}$, WTi, Ni, Si, Cu	$13\times2\times0.5$ mm^3	32.5	3.47	9.8	1 kHz/N	0~10 N
Wu *et al.* [67]	2013	15 pF	2.2 μH	--	PDMS	$83\times5.5^2\pi$ mm^3	22	--	--	73 kHz/0.01ε	0~0.08

Nominal values of the sensors are listed, D denotes the interrogating distance, and k denotes the coupling coefficient.

TABLE IV
TEMPERATURE SENSORS

Reference	Year	C	L	D	Materials	Dimensions	f (MHz)	Q	Re(Z_{in}) (Ω)	Resolution	Sensitivity	Range (°C)
Wang *et al.* [68]	2008	0.24 nF	0.68 μH	2.5 cm	ceramic	Diameter 28.5 mm	10	--	6	--	--	0~235
Marioli *et al.* [69]	2010	22.1 pF	255 μH	A few cm	Si and Al	$50^2\times0.63$ mm^3	--	--	172	--	60 fF/°C	30~330
Woodard *et al.* [71]	2010	--	20.268 μH	--	Piezo ceramic	10^2 cm^2	17.136	--	--	1°C	-16.97 kHz/°C	21~210
Tan *et al.* [72]	2014	11.76 pF	1.345 μH	10 mm	Ferroelectric ceramic	$36^2\times0.68$ mm^3	--	28.8	--	--	-5.75 kHz/°C, -16.67 kHz/°C	25 ~430, 430~700
Ren *et al.* [73]	2014	--	--	--	Graphene oxide	Diameter 10 mm	--	--	--	--	59.3 kHz/°C 46.1 kHz/°C	-40~0, 0~60
Li *et al.* [74]	2015	--	--	1cm	Alumina ceramic	3.7^2 cm^2	27.6	78		1°C	~2 kHz/°C	25~1000

Nominal values of the sensors are listed, D denotes the interrogating distance, and k denotes the coupling coefficient.

The sensitive capacitor comprised steel wires and rubber inside the tires which is served as the electrodes and dielectric material, respectively. Tires deformation changed space between the steel wires, which consequently changed the capacitance. Then in 2007, they proposed a train sensor for the tires based on flexible polyimide substrates [26]. A prototype strain sensor made on polyimide substrate was proposed [66], which was constructed from a planar spiral inductor and an interdigital capacitor. The sensing principle was based on the deformation of the electrodes and the gaps in between. Ferromagnetic magnetostrictive materials show dimensional and magnetization change in response to magnetic fields and mechanical stresses. Based on these ideas, a planar coil on top of a magnetostrictive Galfenol layer was manufactured to monitor the healing process of bone fractures [31]. The inductance would change in response to the bending of the sensor to achieve a shift in its resonant frequency. The serpentine helical inductor encapsulated by materials with high Poisson's ratio was also used to monitor strain [67]. The cross-section area of the helical coil would have more evident change due to lower radial rigidity when an axial deformation was applied.

C. Temperature Sensor

The progress on this area is summarized in Table IV. The monitoring of bearing structure damage and function failure is required for temperature sensors in high temperature environment. This cannot be satisfied by the traditional temperature sensors because of the physical connections and power supply. Hence the *LC* type temperature sensors draw more and more attention due to its passive wireless interrogation, simple structure, and high reliability.

A novel high-K temperature sensitive ceramic material was applied as the sensitive dielectric to test temperature of a rotating component up to 235°C [68]. Instead of using a sensitive dielectric, Marioli *et al.* [69] and Andò *et al.* [70] developed an interdigital sensitive capacitor based on the displacement of the conductive electrodes. A V-shaped bent beam responded to the ambient temperature by inducing a thermal expansion of the structure to cause the displacement of the comb electrodes. Through employing piezo ceramic as a sensing material in a spiral inductor to form an open circuit without electric connections, a novel temperature sensor was developed at NASA which was still able to function even when the sensor was damaged [71]. A temperature sensor fabricated by LTCC technology can operate up to 700°C by using a ferroelectric ceramic as the sensing dielectric [72]. Graphene oxide is also a kind of temperature sensitive material, which was utilized to realize a temperature sensor ranging from −40 °C to 60 °C [73]. The temperature measurement was upgraded to 1000°C by using high-temperature

TABLE V
HUMIDITY SENSORS

Reference	Year	C	L	D	Materials	Dimensions	*f* (MHz)	Re(Z_{in}) (Ω)	T(˚C)	Resolution	Sensitivity	Range (%RH)
Ong *et al.* [20]	2000	--	--	--	TiO_2	4^2 cm^2	23.49	--	23.5	--	8 kHz/%RH	2~98
Harpster *et al.* [75]	2002	180 pF	20 μH	2 cm	Polyimide, NiFe, Cu	7×1.2×1.5 mm^3	4	9.655	37	±2.5%RH	8 kHz/%RH	20~80
Harpster *et al.* [27]	2002	32 pF	2.2 μH	1 cm	Polyimide, Cu, and Si	1.5×0.5×8 mm^3	18.07	54.33	25/37/50	±1.7%RH	4~16 kHz/%RH	30~70
Tan *et al.* [76]	2007	15.7 pF	2.86 μH	--	Paper, Cu	--	~24	--	24	--	13 kHz/%RH	2~65
Ong *et al.* [77]	2008	14.45 pF	2.95 μH	6 cm	Cu	4^2 cm^2	23.04	~30	--	--	--	0~12
Marioli *et al.* [78]	2008	1.75 pF	96.47 μH	30 mm	PEG	Diameter 50 mm	--	30	22	--	6.7 fF/%RH	15~90
Wang *et al.* [79]	2012	7 nF	70 μH	3 mm	Ag, Al, Dupont 5018	100^2 mm^2	0.24	268	23	--	-1.1 kHz/%RH	10~90
Saucer *et al.* [80]	2014	--	--	40 mm	NaCl, paper, Cu	15^2×3.2 mm^3	~10	--	40	--	--	30~90
Deen *et al.* [81]	2014	~80 pF	645 nH	k= 0.16	Graphene, Cu	--	--	--	23	--	5.7 kHz/% RH	1~97
Zhang *et al.* [82]	2014	--	--	--	Polyimide, Al	6^2 mm^2	74		25	--	65 kHz/%RH	10~95
Zhang *et al.* [44]	2015	31.8 pF	0.525 μH	5 mm	GO, Cu	--	36.2	~30	25	--	−18.75 kHz/%RH	15~95
Feng *et al.* [83]	2015	--	--	0.5 cm	Paper, polyimide, PET	40^2 mm^2	157	--	25	--	370 kHz/%RH	20~90
Fernandez -Salmeron *et al.*[84]	2015	30 pF	4.6 μH	--	Polyimide, Ag	--	13.56	650	10~95	--	-3.7 kHz/%RH	15~95

Nominal values of the sensors are listed, D denotes the interrogating distance, and k denotes the coupling coefficient.

co-fired ceramic (HTCC) technology with an alumina ceramic substrate [74].

D. Humidity Sensor

The progress on this area is summarized in Table V. Humidity monitoring is required in many fields such as industry, agriculture, meteorology, and food package. However, traditional humidity sensors cannot apply in some particular situations such as food package, package impermeability, and structure internal monitoring where the wired connection for signal and power is impossible and long term operation is expected without new replacement. *LC* passive wireless sensing technology is very suitable for these situations for its wireless interrogation, small size and simple structure without battery supply.

A small passive wireless humidity sensor was proposed by Harpster *et al.* [75] to present long term performance for implantation. The *LC* type sensor was constructed from a sensitive capacitor based on polyimide and a solenoidal inductor. A ferrite core was employed to improve the readout range up to 2 cm. They then fabricated a planar electroplated copper coil on a polyimide film without an external capacitor to achieve a simple structure and decreased size [27]. Ong *et al.* have made a series of researches on the *LC* sensors. The *LC* sensor used for environment monitoring including humidity test was proposed in 2000 [20]. A planar inductor and capacitor printed on a paper substrate was proposed for quantifying package food quality in 2007 [76]. An embedded sensor for water content in civil engineering materials was also presented [77]. Since the dielectric constant of water was much higher than that of the test sample such as sand and concrete, the presence of water increased the capacitance of the *LC* circuit. Marioli *et al.* developed a humidity sensor, in which a planar spiral fabricated in Print Circuits Board (PCB) technology, based on polyethylene glycol (PEG) as a humidity sensitive material [78]. To further reduce the production cost, an all-printed humidity label was fabricated by an inexpensive and reel-to-reel processing technology based on screen-printing and dry-phase patterning [79]. The irreversible salt deliquescence phenomenon was exploited through monitoring the relative humidity threshold based on a double layer planar coil [80]. The salt distribution process was sensitive to the relative humidity, which permanently altered its permittivity and therefore the arrangements capacitance and the resonant frequency. Graphene is one of the most intensively investigated materials today, and its quantum capacitance effect was developed as a humidity sensitive capacitor [81]. Absorbed water on the graphene surface increases the hole concentration in the already slightly p-type graphene. The increasing hole concentration shifts the Fermi-level further from the

TABLE VI
BIOCHEMICAL SENSORS

Reference	Year	C	L	D	Materials	Dimensions	*f*(MHz)	Q	Re(Z_{in}) (Ω)	Sensitivity	Range
Ong *et al.* [85]	2002	--	--	8 cm	polyurethane	4^2×0.05 cm^2	~17	--	0.7	--	0~1.4×10^7 cfu/mL
Strong *et al.* [89]	2002	--	0.56 μH		Si, hydrogel	4.3^2 mm^2	--	--	--	66 Hz/μmol	0~3 mol/L
Garcia-Canton *et al.* [93]	2007	220 pF	--	1 cm	SiO^2/Si^3N^4, Ag/AgCl	9×4.5^2π mm^3	0.121	>15	--	1 kHz/pH	pH 2-12
Sridhar *et al.* [90]	2009	38.3 pF	1252 nH		Hydrogel, Cu	$10^2$$mm^2$	25	--	--	~10 kHz/pH	pH 2-7
Lei *et al.* [91]	2009	--	2.82 μH	1 mm	Hydrogel, Cu, glass	5^2×0.7mm^3	49.8	--	--	1.16 MHz/pH	pH 2-7.4
Horton *et al.* [28]	2011	330 pF	5.3 μH	6 cm	Ag, Sb, KCl	84×42 mm^2	14.5	--	--	166 kHz/pH	pH 4-10
Bhadra *et al.* [29]	2011	35 pF	28.91 μH	12 cm	Cu	Diameter 6.7cm	5	--	0.6	73 kHz/pH	pH 2-12
Bhadra *et al.* [86]	2014	35 pF	0.13 μH	3 cm	Glass, AgCl	20×6 mm^2	78	55.5	2.5	2.477 MHz/pH	pH 2-12
Perveen *et al.* [87]	2014	39 pF	20.33 μH	8 cm	Glass,Cu	80×35 mm^2	5.9	84.51	2.5	1.2 kHz/mV	-250~450mV
Song *et al.* [92]	2014	--	--	--	Hydrogel, polystyrene beads, Cu	12^2×0.5 mm^3	--	--	--	~2 MHz/pH	pH4~6
Mannoor *et al.* [34]	2012	--	--	--	Silk, Graphene	--	~105	--	20	--	(2~8)×$\log_{10}$ cfu/mL
Bhadra *et al.* [88]	2015	35 pF	20.33 μH	6 cm	AgCl, Ta_2O_5, IrO_2, hydrogel	--	6	--	1	--	1.5~200 ppm

Nominal values of the sensors are listed, D denotes the interrogating distance, and k denotes the coupling coefficient.

Dirac energy, increasing the capacitance and thus decreasing the resonant frequency of the *LC* tank. Zhang *et al.* stacked two counter-rotating planar inductors separated by a maskless polyimide film [82]. The two inductors were inductively and capacitively coupled together to form a resonant tank. They proposed a planar spiral inductor connected with an interdigital capacitor based on graphene oxide (GO) as the sensing material afterwards [44]. A fully-printed chipless humidity tag was presented [83] with different substrates of paper, polyimide, and PET in order to compare their performances. A similar printed humidity sensor was proposed for two different approaches: one for threshold tag including an RFID and the other for humidity monitoring [84]. The inductor was screen printed and the capacitor was inkjet-printed in two different structures with interdigital electrodes and serpentine electrodes.

E. Biochemical Sensors

The progress on this area is summarized in Table VI. Biochemical sensors have been designed for monitoring parameters of interest such as bacteria growth, pH value, concentration of glucose, and antigens, etc.. Among the biochemical sensors for *in vivo* and *in vitro* applications, the *LC* passive wireless sensors present advantages of working without wires in miniature invasion, continuous and long-term monitoring, and reduced dimensions.

The most common applications of biomedical sensors contain the bacterial test and pH monitoring. For the bacterial test, Ong *et al.* utilized an interdigital capacitor and a spiral inductor printed on a thin plastic or paper substrate with a thin polyurethane layer coated on it to monitor bacteria growth in milk, beer, and meat [85]. The effective relative complex permittivity of the biological medium and polyurethane would respond to the bacteria growth, resulting in a resonant frequency shift. Besides, Graphene is capable of detecting analyte with high sensitivity due to its nanoscale nature, and it has thus become another hot material. By printing the resistive graphene monolayer to the silk substrate, the *LC* sensor was implemented for tooth enamel test [37]. The change in conductance of the graphene *LC* sensor is resolved from variation in the characteristic frequencies and bandwidth of sensor resonance.

In the case of pH monitoring, the most common technique is the electrochemical method, which generally consists of electrodes that generate an electrical potential proportional to the pH level of the test solution. Ong *et al.* applied an antimony sensing electrode and a silver reference electrode as the pH electrodes to detect the pH value [28]. Varactors were used serve as the voltage controlled capacitor to respond to the pH change. Bridges *et al.* used an *LC* resonator composed of an inductive coil and a varactor diode to monitor pH with a solution of 0.1pH [29]. After that, they improved the accuracy to 0.08pH and scaled down the sensor size to fit inside a small bioreactor or test tube for fluid embedded applications [86]. They also used the varactor-combined *LC* sensor to detect the corrosion of steel-reinforced concrete civil infrastructure [87].

TABLE VII
GAS SENSORS

Reference	Time	C	L	D	Materials	Dimensions	f(MHz)	Q	Re(Z_{in}) (Ω)	Temperature	Sensitivity	Range
Ong *et al.* [95]	2002	--	--	15 cm	MWNT, SiO_2	2^2×1cm^3	18.4	--	~6	23˚C	-0.0004043 /%CO_2	0~100%
Birdsell *et al.* [96]	2006	9.48 μF	--	--	Ceramic, Al_2O_3,Ba TiO_3-La_2 O_3	50^2 m^2	~42	--	--	--	0.007 ˚/%CO_2	10~100%
Ma *et al.* [97]	2015	--	--	--	SnS_2, Ceramic	25.2^2×0.98 mm^3	21.42	--	--	--	--	77~1155 ppm

Nominal values of the sensors are listed, D denotes the interrogating distance, and k denotes the coupling coefficient.

The resonant frequency changed owing to the corrosion potential produced by two electrodes connected across the varactor. Furthermore, by combing the varactor with the hydrogel, they realized an acidic and basic volatile concentration sensor [88]. The hydrogel coated pH sensitive electrode was connected to the varactor in parallel. Upon absorption of the acidic basic volatiles the hydrogel pH changes, which causes the voltage across the electrode pair to change and shift the resonant frequency as a result. Hydrogel is sensitive to environmental parameters like humidity, temperature, and pH, and it deforms in response to the external excitations. Based on this principle, a hydrogel-actuated *LC* sensor was developed for biosensors [89]. The biosensitive hydrogel between the electrodes of a variable capacitor swelled when exposed to analyte concentration, and exerted contact pressure on the deformable conducting diaphragm to produce a capacitance change. In [90], a hydrogel was sandwiched by a folded coplanar dual spiral coil. The mutual inductance between the two aligned coils was dependent of the gap, which was modulated by the hydrogel. Ziaie *et al.* proposed a stimuli-sensitive hydrogel confined between a stiff porous membrane and a thin glass to form a variable pressure capacitor in order to detect pH [91]. They have also reported a chemical sensor by embedding superparamagnetic nanoparticles into the hydrogel and laminating the hydrogel on a planar coil [92]. The swelling of the hydrogel changed the permeability of the coil to cause the inductance to change. Besides the hydrogel, an electrolyte-insulator-silicon (EIS) capacitor is capable of converting pH to capacitance as well [93]. To achieve a high Q factor, a double-electrode scheme was developed [94]. In addition to the reference electrode, the second electrode is a low resistance electrode and consists of a set of parallel polysilicon tracks that are interdigitated with another set of EIS capacitor strips.

F. Gas Sensor

The progress on this area is summarized in Table VII. Gas sensors are used in many fields, such as industry process like combustion engine environment, climate, human health monitoring, and food and medicine packages as a means of detecting spoilage.

Ong *et al.* proposed an *LC* type gas sensor for CO_2, O_2, and NH_3 [21], [95]. The multiwall carbon nanotube (MWNT)–silicon dioxide (SiO_2) composite layer worked as a gas-responsive material, whose relative permittivity and the conductivity would change when the sensor was exposed to various gases. By extending a temperature sensor fabricated by LTCC technology, the CO_2 sensor was introduced to work at higher temperature [96]. Different concentrations would affect the impedance phase angle value when in measurement. The gas sensor, which was also fabricated by the LTCC technology, was introduced based on SnS_2 to detect different gases including NO_2, EtOH, and NH_3 [97].

G. Other Applications

A reduction of instrumentation mass and volume in ground testing, air flight, and space exploration applications is desired for NASA [98]. Vehicle health monitoring (VHMS) system is designed to ensure the safety of crew and the vehicles. *LC* passive wireless sensors are very suitable for the harsh environment surrounding aerospace vehicles, with temperature extremes ranging from cryogenic to very high for hypersonic vehicles experiencing aerodynamic heating due to skin friction [99].

An *LC* tag used for smart diapers was developed based on a variable capacitor, which was sensitive to the wetting of the diaper [100]. The fluid level can also be detected by using the structure proposed in [71] and the experiment results were demonstrated [101].

For dosage verification and quality control in radiation oncology, the measurement of ionizing radiation within an irradiated solid tumor is extremely valuable. Hence, a wireless implantable microdosimeter was presented based on the decay of surface change of an electret upon exposure to radiation [102]. Another way is to utilize a fully-depleted silicon-on-insulator (FDSOI) variable capacitor as the radiation dosimeter for cancer therapy [103].

A novel inertial switch using multiwall carbon nanotube (MWCNT)-hydrogel integrated with an *LC* tank was presented [104]. When the acceleration exceeds the designed threshold level, the water droplet passes through the channel to the hydrogel cavity, causing the hydrogel to swell and change the capacitance of the *LC* tank. The similar switch structure was employed as a resettable fall-down recorder by replacing the water droplet as a magnetic droplet [105]. After triggering, the switch can be remotely reset to the initial state by an external magnet. To detect the absolute position in rough industrial environments, a rectangular antenna and

TABLE VIII
OTHER APPLICATIONS

Reference	Year	Application	C	L	D	Materials	Dimensions	f	Q	Sensitivity	Range
Yambem *et al.* [100]	2008	Diapers	--	3.1 μH	10 cm	--	4^2 cm^2	12 MHz	--	--	--
Son *et al.* [102]	2008	Radiation	--	11 μH	1.2 cm	Teflon, glass	$28\times1.25^2\pi$ mm^3	26.4 MHz	7	49 kHz/Gy	0~30 Gy
Woodard *et al.* [101]	2010	Fluid-leve	--	--	3.8 cm	--	23^2 cm^2	12 MHz	--	76.8~90.5k Hz/cm	0~25 cm
Kuo *et al.* [104]	2013	Inertial switch	2.08 pF	--	3 mm	Hydrogel, MWCNT, PDMS	15×10×1.5 mm^3	164 MHz	--	--	--
Li *et al.* [103]	2014	Radiation	1.46 fF/μm	--	--	Si	--	1 GHz	>20	--	0~160 Gy
Huang *et al.* [105]	2015	Fall-down recorder	51.27 nF	21.39 μH	3 cm	Cu, Polypropylene	4.7^2 cm^2	151.96 kHz	--	--	0.79~1.24 G
Aschenbrenner *et al.* [106]	2015	Position	--	--	2 mm	--	20×22 mm^2	1 MHz	--	--	0~390 mm

Nominal values of the sensors are listed, D denotes the interrogating distance, and k denotes the coupling coefficient.

a passive *LC* resonant circuit formed a position sensor [106]. The induced voltage in the *LC* target was dependent of the position along the measurement axis and the relative speed between the target and the antenna.

The progress on these applications is summarized in Table VIII.

IV. CHALLENGES AND PROSPECTS

A great deal of progress has been made during past decades to advance an *LC* passive wireless sensor towards a wireless sensing platform. For emerging implantable, wearable, and portable devices as well as Internet of Things, however, challenges remain which include: To form the *LC* sensors for implantable devices by using biodegradable materials, to produce them for wearable devices on flexible substrates, to increase the interrogation distance, and to expand them to multi-functions. This section will address an attempt that has been made towards these directions.

A. Emerging Applications and Challenges

1) Biodegradable Materials for Implantable Devices: Implantable devices have been used for disease monitoring and health care, and more and more researches are focused on the implantable biosensors. The introduction of reliable low cost wireless technology has significantly changed the medical industry over the past decade [107]. An *LC* passive wireless sensor has provided its advantages of long-term work, small size, and battery-free features in the biomedical implantation. For chronic disease states, long- term, permanent sensors are of interest, while for acute disease states, biodegradable wireless microsystems may be of interest [108]. Key to the success of all implantable sensors is the need to ensure reliable performances when exposed to living tissue and fluids [109], hence, the biocompatible material is very essential. Biodegradable performance is another concern of the *LC* implantable sensors. Partially or even fully biodegradable *LC* biosensors are proposed to avoid a second surgery to remove the implant after its period of use. The available materials include conventional biodegradable polymers such as polymers poly (L-lactide) (PLLA) and polycaprolactone (PCL), biodegradable metals such as Mg, Fe and their alloys, and biodegradable conductive polymer composites [110]. The challenges for fabricating the biodegradable *LC* sensors concern the development of new biodegradable materials with adequate conductivity, which attempts to achieve high quality factor Q and low power dissipation in the surrounding tissues. Another issue is the implementation of high-precision fabrication processes with low impact on material properties, which is aimed at large scale production. Besides, the development of characterization procedures adapted to particular components and the evaluation of the DC and RF material properties for circuit design should also be considered.

2) Flexible Substrate for Portable and Wearable Devices: Integrating with smartphone is another development direction for the *LC* sensors. These portable devices are capable of realizing a convenient detection of cough, irregular heartbeat detection, lung function analysis, blood pressure, and *etc*. The corresponding wellness apps can also be processed to assist the sensors, which can lead to early detection to ultimately reduce healthcare costs [111]. In addition, chemical sensing is in the monitoring scope of the smartphone sensors as well [112]. Similar to smartphone, wearable devices like smart watches and smart bands are also very promising. These portable devices are fabricated on a flexible substrate with low production cost to realize the wearable characteristics and mass volumes.

LC passive wireless sensors have also a potential in intelligent packaging for food. The sensors for food quality and safety require them to provide an unobtrusive form, battery-free operation, and minimal cost [113]. The sensors not only monitor the food spoilage to reduce hazard, but also clarify

the main factors in food wastage during supply chain [114]. In the application of food intelligent package, the low cost and flexible substrate like paper are the primary factors, and the development of printing technology [79] and 3D additive manufacturing [115] is very promising in the future.

3) Challenges: An *LC* passive wireless sensor with multifunction is required with the development of implantable, wearable, and portable devices as well as Internet of Things. Monitoring multiple parameters simultaneously sets a high demand for the *LC* sensing. Integrating with a CMOS circuit becomes the general method. A wireless microsystem for pressure, temperature, and relative humidity was presented in [116]. The wireless system was composed of two subsystems: the primary transceiver system and the secondary microsystem. The primary system transmitted power and received load-modulated data through a loosely coupling between the primary and secondary inductors. The secondary inductor was configured as an *LC* oscillator from which a voltage was rectified and regulated to provide a voltage source to the sensor interface. Moreover, using the developed CMOS technology and combining with signal processing, decision capability, and wireless network capability, multifunctional sensors will implement the wireless integrated network for health care, environmental monitoring, and safety and security [117].

Small size requires a miniature dimensions for the entire sensor structure including the antenna coil. However, reducing coil size has a strong impact on the interrogating distance. Simultaneous detection for multiple parameters is limited by the *LC* inherent operation principle.

B. Interrogation Distance

The interrogating range is one of the important factors for *LC* passive wireless sensors. The readout performance is affected by the distance for the magnetic field signal as

$$\frac{P_{received}}{P_{transmitted}} = \frac{G_t G_r}{4}\left(\frac{1}{(kd)^2} + \frac{1}{(kd)^4}\right) \tag{39}$$

where G_t and G_r are the gains of the transmit and receive antennas, respectively, along the specific direction that links them, k is the wave number and d is the straight-line distance between the two antennas [118]. Power received would decrease when distance grows. Several methods have been attempted to enhance the readout distance when the signal intensity received remains the same.

1) Inductor: Increasing the size of an inductor can effectively enhance the magnetic coupling between the readout coil and the sensor inductor according to Eq.(37), which extends the interrogating distance as a result. However, this method increases the chip size which should be avoided in the sensor design. Stacking the two inductors up, which forms a dual-layer inductor as shown in Fig. 5, can handle this problem to some extent while it still achieves a large inductance [119]. There can be electrical connections between the multilayer inductors to form a cohesive whole inductor [120], [121], and the electrical connections can also be absent by using the mutual inductance to integrate them all [82]. However, for higher frequencies, the parasitic interwinding capacitance of the readout coil must also be taken into account.

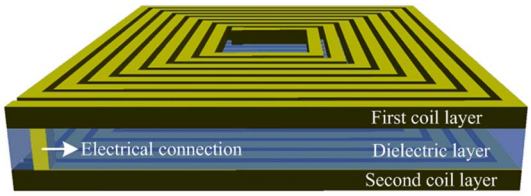

Fig. 5. Configuration of a dual-layer inductor.

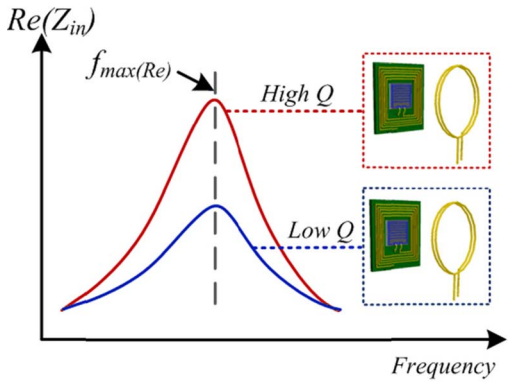

Fig. 6. An *LC* sensor with a high Q factor can achieve a longer readout distance than its counterpart with a low Q factor when the signal intensity keeps the same.

2) Coupling: Adding a ferrite core in the central of the inductor can confine magnetic field to realize a stronger coupling between the interrogating coil and the sensor inductor, and hence achieving a longer interrogating distance. The ferrite core can dramatically increase the inductance when compared with an air core as demonstrated in [75] and [122]. However, the appearance of a ferrite will enlarge the equivalent resistance of the inductor [123], which is adverse to the Q factor improvement of the *LC* sensor [124].

3) Sensitivity and Q Factor: According to the input impedance in Eq.(7), improving Q factor is able to increase the $Re\,(Z_{in})$ to obtain a longer readout distance when the signal intensity remains the same. A sharper peak will appear when an impedance analyzer is used for measuring an *LC* sensor with a higher Q factor. Because of the same signal intensity/$Re\,(Z_{in})$ in measurement, the readout distance of the *LC* sensor with higher Q factor is longer than its counterpart with lower Q factor which is illustrated in Fig.6. As the distance grows, the Q becomes sharper the signal-to-noise goes down. Improving the sensitivity contributes to the signal-to-noise, which also enhances the interrogating distance.

4) Signal Extraction: The measurement in time domain stated in Section II has a wider range than the measurement in frequency domain which is generally used. Despite of its long interrogating range, the measurement in time domain has a strict requirement for the test terminal. For the measurement in frequency domain, the maximum real part and minimum phase dip of the equivalent input impedance are both available

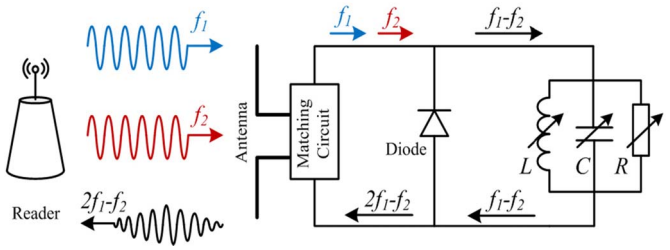

Fig. 7. The operation principle of the intermodulation sensor system.

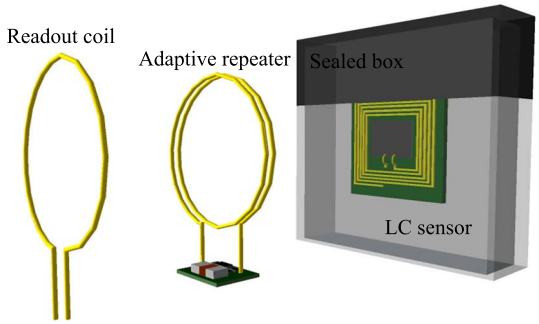

Fig. 8. The representation of "antenna-adaptive repeater-*LC* sensor" model.

for testing, while of which the phase dip method is dependent of the interrogating distance, as shown in Eq.(14). A distance compensated telemetric sensor system was developed based on the phase-dip method [125]. As the interrogating distance grows, it results in a strong decrease of the coupling coefficient k. For very low values of the coupling coefficient, changes in the reflected impedance are smaller than those from the inductance L_0. And Z_{in} argument cannot reach zero, and therefore the resonant frequency of the sensor cannot be determined. An anti-resonance cancellation approach was proposed [126], which may increase the interrogating distance to some extent. A real-time capacitance estimation methodology was also developed by adopting a frequency domain transfer function approach [127], which estimates the capacitance change in real-time by algebraically manipulating two measurements (the magnitude and the phase of the reflected sensor impedance).

Signal transmitting of an *LC* sensor is based on the inductive coupling between the readout coil and the sensor inductor. Compared with electromagnetic (EM) coupling, the inductive coupling range is limited but it allows more sophisticated functionality with sufficient power, whereas EM coupling has a longer detection distance but it has a tight power budget [128].

Adding a varactor diode to the *LC* tank forms a hybrid passive wireless sensor which is interrogated in an intermodulation technique. The sensor also contains an antenna and a matching circuit. As shown in Fig.7 [129], the reader transmits two signals at different frequencies to actuate the sensor, which are mixed in the varactor diode generating current at a difference frequency. The current at the difference frequency then generates a voltage depending on the circuit impedance. This voltage is then further mixed with the original input frequencies to generate intermodulation signals. The resonant circuit contains the sensor element that affects the impedance, and thus the voltage at the difference frequency. The sensor data is finally read out by recording the intermodulation response of the sensor. An optimized sensor was presented in [130] and achieved a 13m-distance when the sensor capacitance changed in 1%. The corresponding algorithm was developed as well to estimate the quantity measured by the wireless senor from its intermodulation response [131]. Another modulation communication is based on a single carrier frequency for ultra-high-frequency RFID (radio frequency identification) applications. The readout distance of the implemented sensor can reach up to 14m [132].

5) Repeater: Adding an additional resonant repeater/relay, which works as a receiver and a relay in the magnetic field, would enhance the magnetic coupling over a longer distance. This scheme has been proposed and demonstrated in wireless power transfer (WPT) for midrange applications [133], [134]. When used in passive wireless sensor detection, the repeater also operates in passive manner and can enhance the readout [135]. A passive resonator was used for *LC* sensor readout enhancement. The *LC* interrogating system with a resonant repeater was analyzed theoretically including phenomenon of frequency splitting and sensitivity decay [136]. The resonant repeater with a fixed resonant frequency is limited in enhancing the sensor signal only around its own resonant frequency, while it is not capable of the entire range of the *LC* sensor. This approach was optimized by using a cyclic-scanning repeater, whose resonant frequency was cyclic-scanned so as to detect that of the *LC* sensor. As shown in Fig.8, the cyclic scanning was realized by a voltage-dependent varactor, and this method can solve the sensitivity decay mentioned above [137]. A fully passive system was further proposed by using an adaptive repeater in [138]. Fig.8 shows the schematic representation of this "antenna-adaptive repeater-*LC* sensor" topology. The resonant frequency of the passive wireless adaptive repeater is cyclic-scanning within a frequency spectrum which covers the full range of the sensor operating resonant frequency. When the resonant frequency of the repeater becomes consistent with that of the sensor, the strong magnetic coupling occurs. The resonant frequency of the passive wireless adaptive repeater was cyclic-scanned changed by a controlled voltage which is induced by itself through coupling from the readout coil. Other repeater like magneto-inductive-waveguide [139] can also be considered as an approach to extend the energy transmitting.

C. Multifunction

Several efforts have been made to expand an *LC* passive wireless sensor to multi-functions.

1) Resonant Frequency and Q Factor: For an *LC* sensor, the detected results include the resonant frequency and the amplitude of $Re\,(Z_{in})$ or Q factor [140]. These two factors both reflect the sensing elements according to Eqs.(7) and (8), thus extracting them can realize a double-function. In the tire pressure monitoring system [35], a pressure sensitive capacitor was connected with a temperature sensitive inductor. The applied pressure affected the resonant frequency while the temperature affected the bandwidth and amplitude of the impedance at the frequency. After that, the pressure sensor with temperature compensation was proposed [141], where the pressure shifted

TABLE IX
MULTIFUNCTIONAL SENSORS

Reference	Year	C	L	D	Materials	Dimensions	*f* (MHz)	Q	Re(Z_{in}) (Ω)	Parameter	Sensitivity	Range
Nabipoor *et al.*[35]	2006	--	--	--	Si, glass, Al	6^2 mm^2	56	--	--	Pressure	194.8 kHz/psi	0~100 psi
										Temperature	0.273 Ω/˚C	-100~300 ˚C
Rocznik *et al.* [141]	2012	--	--	3 mm	Si	--	100	6	--	Pressure	--	1~3 Bar
										Temperature	--	-40~140 ˚C
Zhang *et al.* [142]	2012	39.3 pF	0.266 μH	1 cm	Au, SU-8	2^2 cm^2	63.02	23.45	5.9	Dielectric constant	--	1~80
										Conductivity	--	--
Bhadra *et al.* [36]	2013	35 pF	2.1 μH	8.5 cm	Ag/AgCl, Cu	4×3 cm^2	18	54	--	pH	174 kHz/pH	pH 1.5~12
										Temperature	-2.61/˚C	25~55 ˚C
Ren *et al.* [143]	2015	40 pF	0.56 μH	k= 0.125	GO, Al, Cu	10^2 mm^2	36.36	--	1214.95	Humidity	-17.8 kHz/%RH	55~95 %RH
										Temperature	-6.27 Ω/˚C	10~40 ˚C

Nominal values of the sensors are listed, D denotes the interrogating distance, and k denotes the coupling coefficient.

the resonant frequency by a MEMS sensitive capacitor and the temperature affected the Q factor of the sensor. For environmental monitoring, a chemical sensor based on the change of dielectric constant and conductivity was introduced [142]. The distributed capacitance and conductance of the sensor were affected by the dielectric constant and conductivity, which is reflected in the resonant frequency and the phase dip so as to provide information about the surrounding environment. For the electrode-based pH sensors, the temperature must be accounted for in order to provide accurate measurements. Bhadra *et al.* employed a temperature-dependent resistor to provide the temperature compensation [36]. The temperature dependent resistance change was detected by the Q factor, and the pH variation was reflected in the resonant frequency. A method to extract the both temperature and humidity was also proposed, which was based on the measurement of the resonant frequency and the real portion magnitude maximum of the impedance [143].

The progress in this direction is summarized in Table IX.

2) Specific Winding Inductor: Arranging several *LC* sensors in an array makes the multi-parameter monitoring possible. However, this simple construction concerns a vital problem: the large area of the sensor, which is also accompanied with a large readout coil. Stacking the sensors up as mentioned above can solve this problem. However, the mutual inductance is the remarkable factor to be considered. The mutual inductance between the inductors has an influence on the resonant frequency of each *LC* sensor, and an unexpected shift of the resonant frequency would occur due to the mutual coupling. As shown in Fig.9, a specific winding inductor was introduced [144] to achieve the minimized mutual inductance when coaxially aligned stacked in substrate. The mutual inductance was greatly suppressed to make the stacked *LC* sensors respond to multi-parameters independently.

3) On-Chip Passive Switch: As far as a traditional *LC* passive wireless sensor with one inductor is concerned, in order

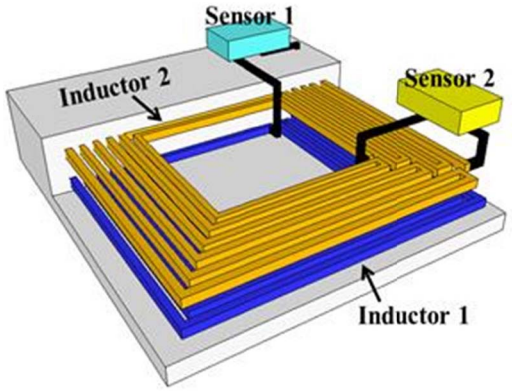

Fig. 9. A 3D model of two staked specific winding inductors connected with two sensors, respectively.

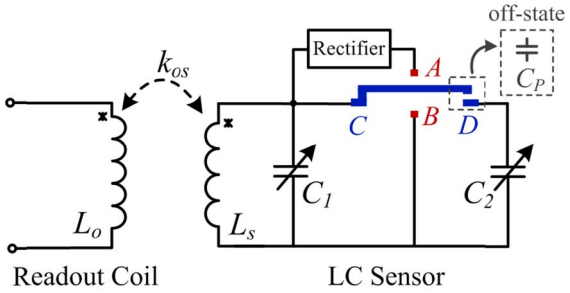

Fig. 10. Schematic circuit of an *LC* double parameter monitoring system integrated with a relay switch.

to monitor multiple parameters, different sensitive elements (sensitive capacitor and resistor) are required to be integrated in the same chip. This basic idea faces only one resonant frequency generated by the inductor, which is impossible to separate the different parameters from each other. Hence, a passive switch such as a typical MEMS switch is available to makes the *LC* sensor work in a sort of time division multiplexing way. As shown in Fig.10, different sensitive

elements are selectively connected to the inductor controlled by the switch to implement a multi-state for detection. This approach was demonstrated to realize a humidity and pressure monitoring by a relay switch via a PCB [145]. All passive components including the inductor, capacitor, and switch integrated on the same chip are being developed. The performance of the switch has a great impact on the whole *LC* sensor, thus choosing the appropriate switch is very important.

V. Conclusions

LC passive wireless sensors have been developed since the 1960's. They have found wide applications in different areas. The manufacturing technologies, such as CMOS MEMS technology, printing technology, and 3D printing technology, etc., flourish for the sensor fabrication. Various materials spring up as well: from the traditional silicon substrate to the flexible substrate such as polyimide and paper, from the traditional sensitive medium such as ceramic to the new sensing material such as GO, MWCNT, and hydrogel. More and more progressive technologies and advanced materials are expected to expand their applications. The passive *LC* wireless sensors with smaller size, longer interrogating distance and more functions continue to evolve in the future.

References

[1] C. C. Collins, "Miniature passive pressure transensor for implanting in the eye," *IEEE Trans. Biomed. Eng.*, vol. BME-14, no. 2, pp. 74–83, Apr. 1967.

[2] L. Rosengren, Y. Backlund, T. Sjostrom, B. Hok, and B. Svedbergh, "A system for wireless intra-ocular pressure measurements using a silicon micromachined sensor," *J. Micromech. Microeng.*, vol. 2, no. 3, pp. 202–204, 1992.

[3] K. Van Schuylenbergh and R. Puers, "Passive telemetry by harmonics detection," in *Proc. 18th Int. Conf. IEEE Eng. Med. Biol. Soc. (EMBS)*, vol. 1. Amsterdam, The Netherlands, Oct. 1996, pp. 299–300.

[4] J. A. Henao-Sepulveda, M. Toledo-Quinones, and Y. Jia, "Contactless monitoring of ball bearing temperature," in *Proc. IEEE Instrum. Meas. Technol. Conf.*, Ottawa, ON, Canada, May 2005, pp. 1571–1573.

[5] S. Scott, A. Kovacs, L. Gupta, J. Katz, F. Sadeghi, and D. Peroulis, "Wireless temperature microsensors integrated on bearings for health monitoring applications," in *Proc. 24th IEEE Int. Conf. Micro Electro Mech. Syst.*, Cancún, Mexico, Jan. 2011, pp. 660–663.

[6] J. Coosemans, M. Catrysse, and R. Puers, "A readout circuit for an intra-ocular pressure sensor," *Sens. Actuators A, Phys.*, vol. 110, nos. 1–3, pp. 432–438, 2004.

[7] J. Xiong *et al.*, "Wireless LTCC-based capacitive pressure sensor for harsh environment," *Sens. Actuators A, Phys.*, vol. 197, pp. 30–37, Aug. 2013.

[8] J. T. Simonen, M. M. Andringa, K. M. Grizzle, S. L. Wood, and D. P. Neikirk, "Wireless sensors for monitoring corrosion in reinforced concrete members," *Proc. SPIE*, vol. 5391, pp. 587–596, Jul. 2004.

[9] L. Schwiebert, S. K. S. Gupta, and J. Weinmann, "Research challenges in wireless networks of biomedical sensors," in *Proc. 7th Int. Conf. Mobile Comput. Netw.*, Rome, Italy, Jul. 2001, pp. 151–165.

[10] A. Zanella, N. Bui, A. Castellani, L. Vangelista, and M. Zorzi, "Internet of Things for smart cities," *IEEE Internet Things J.*, vol. 1, no. 1, pp. 22–32, Feb. 2014.

[11] M. Billinghurst and T. Starner, "Wearable devices: New ways to manage information," *Computer*, vol. 32, no. 1, pp. 57–64, Jan. 1999.

[12] R. Nopper, R. Niekrawietz, and L. Reindl, "Wireless readout of passive LC sensors," *IEEE Trans. Instrum. Meas.*, vol. 59, no. 9, pp. 2450–2457, Sep. 2010.

[13] D. Kajfez and E. J. Hwan, "Q-factor measurement with network analyzer," *IEEE Trans. Microw. Theory Techn.*, vol. 32, no. 7, pp. 666–670, Jul. 1984.

[14] V. Leus and D. Elata, "Fringing field effect in electrostatic actuators," Technion–Israel Inst. Technol., Haifa, Israel, Tech. Rep. ETR 2004-2, 2004.

[15] R. Igreja and C. J. Dias, "Analytical evaluation of the interdigital electrodes capacitance for a multi-layered structure," *Sens. Actuators A, Phys.*, vol. 112, pp. 291–301, May 2004.

[16] U.-M. Jow and M. Ghovanloo, "Modeling and optimization of printed spiral coils in air, saline, and muscle tissue environments," *IEEE Trans. Biomed. Circuits Syst.*, vol. 3, no. 5, pp. 339–347, Oct. 2009.

[17] S. S. Mohan, M. del Mar Hershenson, S. P. Boyd, and T. H. Lee, "Simple accurate expressions for planar spiral inductances," *IEEE J. Solid-State Circuits*, vol. 34, no. 10, pp. 1419–1424, Oct. 1999.

[18] D. G. Fink and H. W. Beaty, Eds., *Standard Handbook for Electrical Engineers*. New York, NY, USA: McGraw-Hill, 1993.

[19] W. B. Kuhn and N. M. Ibrahim, "Analysis of current crowding effects in multiturn spiral inductors," *IEEE Trans. Microw. Theory Techn.*, vol. 49, no. 1, pp. 31–38, Jan. 2001.

[20] K. G. Ong and C. A. Grimes, "A resonant printed-circuit sensor for remote query monitoring of environmental parameters," *Smart Mater. Struct.*, vol. 9, no. 4, pp. 421–428, 2000.

[21] K. G. Ong and C. A. Grimes, "A carbon nanotube-based sensor for CO_2 monitoring," *Sensors*, vol. 1, no. 6, pp. 193–205, 2001.

[22] D. A. Sanz, E. A. Unigarro, J. F. Osma, and F. Segura-Quijano, "Low cost wireless passive microsensors for the detection of hazardous compounds in water systems for control and monitoring," *Sens. Actuators B, Chem.*, vol. 178, pp. 26–33, Mar. 2013.

[23] B. Ando, S. Baglio, N. Pitrone, N. Savalli, and C. Trigona, "'Bent beam' MEMS temperature sensors for contactless measurements in harsh environments," in *Proc. IEEE Instrum. Meas. Technol. Conf.*, Victoria, BC, Canada, May 2008, pp. 1930–1934.

[24] S. Chatzandroulis, D. Tsoukalas, and P. A. Neukomm, "A miniature pressure system with a capacitive sensor and a passive telemetry link for use in implantable applications," *J. Microelectromech. Syst.*, vol. 9, no. 1, pp. 18–23, 2000.

[25] A. DeHennis and K. D. Wise, "A double-sided single-chip wireless pressure sensor," in *Proc. 15th IEEE Int. Conf. Micro Electro Mech. Syst.*, Las Vegas, NV, USA, Jan. 2002, pp. 252–255.

[26] R. Matsuzaki and A. Todoroki, "Wireless flexible capacitive sensor based on ultra-flexible epoxy resin for strain measurement of automobile tires," *Sens. Actuators A, Phys.*, vol. 140, no. 1, pp. 32–42, 2007.

[27] T. J. Harpster, B. Stark, and K. Najafi, "A passive wireless integrated humidity sensor," *Sens. Actuators A, Phys.*, vol. 95, pp. 100–107, Jan. 2002.

[28] B. E. Horton, S. Schweitzer, A. J. DeRouin, and K. G. Ong, "A varactor-based, inductively coupled wireless pH sensor," *IEEE Sensors J.*, vol. 11, no. 4, pp. 1061–1066, Apr. 2011.

[29] S. Bhadra, G. E. Bridges, D. J. Thomson, and M. S. Freund, "Electrode potential-based coupled coil sensor for remote pH monitoring," *IEEE Sensors J.*, vol. 11, no. 11, pp. 2813–2819, Nov. 2011.

[30] M. G. Kisic *et al.*, "Passive wireless sensor for force measurements," *IEEE Trans. Magn.*, vol. 51, no. 1, pp. 1–4, Jan. 2015.

[31] S. Sauer, U. Marschner, B. Adolphi, B. Clasbrummel, and W.-J. Fischer, "Passive wireless resonant Galfenol sensor for osteosynthesis plate bending measurement," *IEEE Sensors J.*, vol. 12, no. 5, pp. 1226–1233, May 2012.

[32] Y.-S. Kim, S.-C. Yu, H. Lu, J.-B. Lee, and H. Lee, "A class of micromachined magnetic resonator for high-frequency magnetic sensor applications," *J. Appl. Phys.*, vol. 99, no. 8, p. 08B309, 2006.

[33] V. Raposo, M. Vázquez, A. G. Flores, M. Zazo, and J. I. Iñiguez, "Giant magnetoimpedance effect enhancement by circuit matching," *Sens. Actuators A, Phys.*, vol. 106, pp. 329–332, Sep. 2003.

[34] J. C. Butler, A. J. Vigliotti, F. W. Verdi, and S. M. Walsh, "Wireless, passive, resonant-circuit, inductively coupled, inductive strain sensor," *Sens. Actuators A, Phys.*, vol. 102, nos. 1–2, pp. 61–66, Dec. 2002.

[35] M. Nabipoor and B. Y. Majlis, "A new passive telemetry LC pressure and temperature sensor optimized for TPMS," *J. Phys., Conf. Ser.*, vol. 34, no. 34, pp. 770–775, 2006.

[36] S. Bhadra, D. S. Y. Tan, D. J. Thomson, M. S. Freund, and G. E. Bridges, "A wireless passive sensor for temperature compensated remote pH monitoring," *IEEE Sensors J.*, vol. 13, no. 6, pp. 2428–2436, Jun. 2013.

[37] M. S. Mannoor *et al.*, "Graphene-based wireless bacteria detection on tooth enamel," *Nature Commun.*, vol. 3, Mar. 2012, Art. no. 763.

[38] M. M. Andringa, D. P. Neikirk, and S. L. Wood, "Unpowered wireless analog resistance sensor," *Proc. SPIE*, vol. 5391, pp. 356–367, Jul. 2004.

[39] S. Sauer and W.-J. Fischer, "A wireless passive humidity threshold monitoring solution based on a permanent resistance change," *Procedia Eng.*, vol. 87, pp. 688–691, Dec. 2014.

[40] M. Soma, D. C. Galbraith, and R. L. White, "Radio-frequency coils in implantable devices: Misalignment analysis and design procedure," *IEEE Trans. Biomed. Eng.*, vol. 34, no. 4, pp. 276–282, Apr. 1987.

[41] B. Liea and K. J. Loh, "Passive wireless sensors for monitoring particle movement at soil-structure interfaces," *Proc. SPIE*, vol. 7647, pp. 76470F-1–76470F-12, Mar. 2010.

[42] J. Joy, J. Kroh, M. Ellis, M. Allen, and W. Pyle, "Communicating with implanted wireless sensor," U.S. Patent 7 245 117, Jul. 17, 2007.

[43] S. T. J. Kaiser, "Passive telemetric readout system," *IEEE Sensors J.*, vol. 6, no. 5, pp. 1340–1345, Oct. 2006.

[44] C. Zhang, L.-F. Wang, J.-Q. Huang, and Q.-A. Huang, "An LC-type passive wireless humidity sensor system with portable telemetry unit," *J. Microelectromech. Syst.*, vol. 24, no. 3, pp. 575–581, Jun. 2015.

[45] B. J. Peterson, A. V. Olson, and T. J. Kaiser, "A wireless sensor interrogator design for passive resonant frequency sensors using frequency modulation spectroscopy," *IEEE Sensors J.*, vol. 10, no. 12, pp. 1884–1890, Dec. 2010.

[46] R. Puers, G. Vandevoorde, D. DeBruyker, R. Puers, and G. Vandevoorde, "Electrodeposited copper inductors for intraocular pressure telemetry," *J. Micromech. Microeng.*, vol. 10, no. 2, pp. 124–129, 2000.

[47] M. A. Fonseca, M. G. Allen, J. Kroh, and J. White, "Flexible wireless passive pressure sensors for biomedical applications," in *Proc. 12th Solid-State Sens., Actuator, Microsyst. Workshop*, Hilton Head Island, SC, USA, Jun. 2006, pp. 37–42.

[48] P.-J. Chen, D. C. Rodger, S. Saati, M. S. Humayun, and Y.-C. Tai, "Microfabricated implantable parylene-based wireless passive intraocular pressure sensors," *J. Microelectromech. Syst.*, vol. 17, no. 6, pp. 1342–1351, Dec. 2008.

[49] P.-J. Chen, S. Saati, R. Varma, M. S. Humayun, and Y.-C. Tai, "Wireless intraocular pressure sensing using microfabricated minimally invasive flexible-coiled LC sensor implant," *J. Microelectromech. Syst.*, vol. 19, no. 4, pp. 721–734, Aug. 2010.

[50] J. Zhai, T. V. How, and B. Hon, "Design and modelling of a passive wireless pressure sensor," *CIRP Ann. Manuf. Technol.*, vol. 59, no. 1, pp. 187–190, 2010.

[51] M. Luo, A. W. Martinez, C. Song, F. Herrault, and M. G. Allen, "A microfabricated wireless RF pressure sensor made completely of biodegradable materials," *J. Microelectromech. Syst.*, vol. 23, no. 1, pp. 4–13, 2014.

[52] N. Xue, S.-P. Chang, and J.-B. Lee, "A SU-8-based microfabricated implantable inductively coupled passive RF wireless intraocular pressure sensor," *J. Microelectromech. Syst.*, vol. 21, no. 6, pp. 1338–1346, Dec. 2012.

[53] G. Chitnis, T. Maleki, B. S. Samuels, L. B. Cantor, and B. Ziaie, "A minimally invasive implantable wireless pressure sensor for continuous IOP monitoring," *IEEE Trans. Biomed. Eng.*, vol. 60, no. 1, pp. 250–256, Jan. 2013.

[54] A. Kim, C. R. Powell, and B. Ziaie, "An implantable pressure sensing system with electromechanical interrogation scheme," *IEEE Trans. Biomed. Eng.*, vol. 61, no. 7, pp. 2209–2217, Jul. 2014.

[55] L. Y. Chen *et al.*, "Continuous wireless pressure monitoring and mapping with ultra-small passive sensors for health monitoring and critical care," *Nature Commun.*, vol. 5, p. 5028, Oct. 2014.

[56] M. Husák, "One-chip integrated resonance circuit with a capacitive pressure sensor," *J. Micromech. Microeng.*, vol. 7, no. 3, pp. 173–178, 1997.

[57] E.-C. Park, J.-B. Yoon, and E. Yoon, "Hermetically sealed inductor-capacitor (LC) resonator for remote pressure monitoring," *Jpn. J. Appl. Phys.*, vol. 37, no. 12B, pp. 7124–7128, 1998.

[58] J. M. English and M. G. Allen, "Wireless micromachined ceramic pressure sensors," in *Proc. 12th IEEE Int. Conf. Micro Electro Mech. Syst.*, Orlando, FL, USA, Jan. 1999, pp. 511–516.

[59] M. A. Fonseca, J. M. English, M. von Arx, and M. G. Allen, "Wireless micromachined ceramic pressure sensor for high-temperature applications," *J. Microelectromech. Syst.*, vol. 11, no. 4, pp. 337–343, Aug. 2002.

[60] O. Akar, T. Akin, and K. Najafi, "A wireless batch sealed absolute capacitive pressure sensor," *Sens. Actuators A, Phys.*, vol. 95, no. 1, pp. 29–38, 2001.

[61] A. Baldi, W. Choi, and B. Ziaie, "A self-resonant frequency-modulated micromachined passive pressure transensor," *IEEE Sensors J.*, vol. 3, no. 6, pp. 728–733, Dec. 2003.

[62] G. Chitnis and B. Ziaie, "A ferrofluid-based wireless pressure sensor," *J. Micromech. Microeng.*, vol. 23, no. 12, p. 125031, 2013.

[63] K.-H. Shin, C.-R. Moon, T.-H. Lee, C.-H. Lim, and Y.-J. Kim, "Flexible wireless pressure sensor module," *Sens. Actuators A, Phys.*, vols. 123–124, pp. 30–35, Sep. 2005.

[64] G. J. Radosavljevic, L. D. Zivanov, W. Smetana, A. M. Maric, M. Unger, and L. F. Nad, "A wireless embedded resonant pressure sensor fabricated in the standard LTCC technology," *IEEE Sensors J.*, vol. 9, no. 12, pp. 1956–1962, Dec. 2009.

[65] R. Matsuzaki and A. Todoroki, "Passive wireless strain monitoring of tyres using capacitance and tuning frequency changes," *Smart Mater. Struct.*, vol. 14, no. 4, pp. 561–568, 2005.

[66] Y. Jia, K. Sun, F. J. Agosto, and M. T. Quiñones, "Design and characterization of a passive wireless strain sensor," *Meas. Sci. Technol.*, vol. 17, no. 11, pp. 2869–2876, 2006.

[67] S.-Y. Wu and W. Hsu, "Design and characterization of LC strain sensors with novel inductor for sensitivity enhancement," *Smart Mater. Struct.*, vol. 22, no. 10, p. 105015, 2013.

[68] Y. Wang, Y. Jia, Q. Chen, and Y. Wang, "A passive wireless temperature sensor for harsh environment applications," *Sensors*, vol. 8, pp. 7982–7995, Dec. 2008.

[69] D. Marioli, E. Sardini, and M. Serpelloni, "Passive hybrid MEMS for high-temperature telemetric measurements," *IEEE Trans. Instrum. Meas.*, vol. 59, no. 5, pp. 1353–1361, May 2010.

[70] B. Andò, S. Baglio, N. Savalli, and C. Trigona, "Cascaded 'triple-bent-beam' MEMS sensor for contactless temperature measurements in nonaccessible environments," *IEEE Trans. Instrum. Meas.*, vol. 60, no. 4, pp. 1348–1357, Apr. 2011.

[71] S. E. Woodard, C. Wang, and B. D. Taylor, "Wireless temperature sensing using temperature-sensitive dielectrics within responding electric fields of open-circuit sensors having no electrical connections," *Meas. Sci. Technol.*, vol. 21, no. 7, pp. 025107-1–025107-11, 2010.

[72] Q. Tan *et al.*, "A harsh environment-oriented wireless passive temperature sensor realized by LTCC technology," *Sensors*, vol. 14, no. 3, pp. 4154–4166, 2014.

[73] Q.-Y. Ren, J.-Q. Huang, L.-F. Wang, S. Wan, L.-T. Sun, and Q.-A. Huang, "Temperature sensing properties of the passive wireless sensor based on graphene oxide films," in *Proc. IEEE Sensors*, Valencia, Spain, Nov. 2014, pp. 432–435.

[74] C. Li, Q. Tan, W. Zhang, C. Xue, and J. Xiong, "An embedded passive resonant sensor using frequency diversity technology for high-temperature wireless measurement," *IEEE Sensors J.*, vol. 15, no. 2, pp. 1055–1060, Feb. 2015.

[75] T. J. Harpster, S. Hauvespre, M. R. Dokmeci, and K. Najafi, "A passive humidity monitoring system for *in situ* remote wireless testing of micropackages," *J. Microelectromech. Syst.*, vol. 11, no. 1, pp. 61–67, Feb. 2002.

[76] E. L. Tan, W. N. Ng, R. Shao, B. D. Pereles, and K. G. Ong, "A wireless, passive sensor for quantifying packaged food quality," *Sensors*, vol. 7, no. 9, pp. 1747–1756, 2007.

[77] J. B. Ong, Z. You, J. Mills-Beale, E. L. Tan, B. D. Pereles, and K. G. Ong, "A wireless, passive embedded sensor for real-time monitoring of water content in civil engineering materials," *IEEE Sensors J.*, vol. 8, no. 12, pp. 2053–2058, Dec. 2008.

[78] D. Marioli, E. Sardini, and M. Serpelloni, "An inductive telemetric measurement system for humidity sensing," *Meas. Sci. Technol.*, vol. 19, no. 11, pp. 115204-1–115204-8, 2008.

[79] X. Wang *et al.*, "An all-printed wireless humidity sensor label," *Sens. Actuators B, Chem.*, vols. 166–167, pp. 556–561, May 2012.

[80] S. Sauer and W.-J. Fischer, "A passive wireless humidity threshold monitoring sensor principle based on deliquescent salts and a diffusion based irreversible state change," *IEEE Sensors J.*, vol. 14, no. 4, pp. 971–978, Apr. 2014.

[81] D. A. Deen, E. J. Olson, M. A. Ebrish, and S. J. Koester, "Graphene-based quantum capacitance wireless vapor sensors," *IEEE Sensors J.*, vol. 14, no. 5, pp. 1459–1466, May 2014.

[82] C. Zhang, L. Guo, L.-F. Wang, J.-Q. Huang, and Q.-A. Huang, "Passive wireless integrated humidity sensor based on dual-layer spiral inductors," *Electron. Lett.*, vol. 50, no. 18, pp. 1287–1289, Aug. 2014.

[83] Y. Feng, L. Xie, Q. Chen, and L. R. Zheng, "Low-cost printed chipless RFID humidity sensor tag for intelligent packaging," *IEEE Sensors J.*, vol. 15, no. 6, pp. 3201–3208, Jun. 2015.

[84] J. Fernandez-Salmeron, A. Rivadeneyra, M. A. C. Rodriguez, L. F. Capitan-Vallvey, and A. J. Palma, "HF RFID tag as humidity sensor: Two different approaches," *IEEE Sensors J.*, vol. 15, no. 10, pp. 5726–5733, Oct. 2015.

[85] K. G. Ong, J. S. Bitler, C. A. Grimes, L. G. Puckett, and L. G. Bachas, "Remote query resonant-circuit sensors for monitoring of bacteria growth: Application to food quality control," *Sensors*, vol. 2, pp. 219–232, Jun. 2002.

[86] S. Bhadra *et al.*, "Fluid embeddable coupled coil sensor for wireless pH monitoring in a bioreactor," *IEEE Trans. Instrum. Meas.*, vol. 63, no. 5, pp. 1337–1346, May 2014.

[87] K. Perveen, G. E. Bridges, S. Bhadra, and D. J. Thomson, "Corrosion potential sensor for remote monitoring of civil structure based on printed circuit board sensor," *IEEE Trans. Instrum. Meas.*, vol. 63, no. 10, pp. 2422–2431, Oct. 2014.

[88] S. Bhadra, D. J. Thomson, and G. E. Bridges, "Monitoring acidic and basic volatile concentration using a pH-electrode based wireless passive sensor," *Sens. Actuators B, Chem.*, vol. 209, pp. 803–810, Mar. 2015.

[89] Z. A. Strong, A. W. Wang, and C. F. McConaghy, "Hydrogel-actuated capacitive transducer for wireless biosensors," *Biomed. Microdevices*, vol. 4, no. 2, pp. 97–103, 2002.

[90] V. Sridhar and K. Takahata, "A hydrogel-based passive wireless sensor using a flex-circuit inductive transducer," *Sens. Actuators A, Phys.*, vol. 155, no. 1, pp. 58–65, 2009.

[91] M. Lei, A. Baldi, E. Nuxoll, R. A. Siegel, and B. Ziaie, "Hydrogel-based microsensors for wireless chemical monitoring," *Biomed. Microdevices*, vol. 11, no. 3, pp. 529–538, Jun. 2009.

[92] S. H. Song, J. H. Park, G. Chitnis, R. A. Siegel, and B. Ziaie, "A wireless chemical sensor featuring iron oxide nanoparticle-embedded hydrogels," *Sens. Actuators B, Chem.*, vol. 193, pp. 925–930, Mar. 2014.

[93] J. García-Cantón, A. Merlos, and A. Baldi, "A wireless *LC* chemical sensor based on a high quality factor EIS capacitor," *Sens. Actuators B, Chem.*, vol. 126, pp. 648–654, Oct. 2007.

[94] J. García-Cantón, A. Merlos, and A. Baldi, "High-quality factor electrolyte insulator silicon capacitor for wireless chemical sensing," *IEEE Electron Device Lett.*, vol. 28, no. 1, pp. 27–29, Jan. 2007.

[95] K. G. Ong, K. Zeng, and C. A. Grimes, "A wireless, passive carbon nanotube-based gas sensor," *IEEE Sensors J.*, vol. 2, no. 2, pp. 82–88, Apr. 2002.

[96] E. Birdsell and M. G. Allen, "Wireless chemical sensors for high temperature environments," in *Proc. 12th Solid-State Sens., Actuators, Microsyst. Workshop*, Hilton Head Island, SC, USA, Jun. 2006, pp. 212–215.

[97] M. Ma, Z. Liu, W. Shan, Y. Li, K. Kalantar-Zadeh, and W. Wlodarski, "Passive wireless gas sensors based on the LTCC technique," in *Proc. IEEE IMWS-AMP*, Suzhou, China, Jul. 2015, pp. 1–3.

[98] W. C. Wilson and P. D. Juarez, "Emerging needs for pervasive passive wireless sensor networks on aerospace vehicles," *Procedia Comput. Sci.*, vol. 37, pp. 101–108, Sep. 2014.

[99] W. C. Wilson and G. M. Atkinson, "Passive wireless sensor applications for NASA's extreme aeronautical environments," *IEEE Sensors J.*, vol. 14, no. 11, pp. 3745–3753, Nov. 2014.

[100] L. Yambem, M. K. Yapici, and J. Zou, "A new wireless sensor system for smart diapers," *IEEE Sensors J.*, vol. 8, no. 3, pp. 238–239, Mar. 2008.

[101] S. E. Woodard, "Functional electrical sensors as single component electrically open circuits having no electrical connections," *IEEE Trans. Instrum. Meas.*, vol. 59, no. 12, pp. 3206–3213, Dec. 2010.

[102] C. Son and B. Ziaie, "A wireless implantable passive microdosimeter for radiation oncology," *IEEE Trans. Biomed. Eng.*, vol. 55, no. 6, pp. 1772–1775, Jun. 2008.

[103] Y. Li *et al.*, "Fully-depleted silicon-on-insulator devices for radiation dosimetry in cancer therapy," *IEEE Trans. Nucl. Sci.*, vol. 61, no. 6, pp. 3443–3450, Dec. 2014.

[104] J.-C. Kuo, P.-H. Kuo, Y.-T. Lai, C.-W. Ma, S.-S. Lu, and Y.-J. J. Yang, "A passive inertial switch using MWCNT–hydrogel composite with wireless interrogation capability," *J. Microelectromech. Syst.*, vol. 22, no. 3, pp. 646–654, Jun. 2013.

[105] C.-Y. Huang, P. Sun, M.-S. Lee, S.-Y. Wu, Y.-C. Shieh, and W. Hsu, "A resettable, wireless and passive fall-down recorder using a magnetic droplet with an *LC* circuit," *IEEE Sensors J.*, vol. 16, no. 3, pp. 654–661, Feb. 2016.

[106] B. Aschenbrenner and B. G. Zagar, "Analysis and validation of a planar high-frequency contactless absolute inductive position sensor," *IEEE Trans. Instrum. Meas.*, vol. 64, no. 3, pp. 768–775, Mar. 2015.

[107] M. R. Mahfouz, M. J. Kuhn, and G. To, "Wireless medical devices: A review of current research and commercial systems," in *Proc. IEEE Topical Conf. Biomed. Wireless Technol., Netw., Sens. Syst. (BioWireleSS)*, Austin, TX, USA, Jan. 2013, pp. 16–18.

[108] M. G. Allen, "Micromachined endovascularly-implantable wireless aneurysm pressure sensors: From concept to clinic," in *Proc. 13th IEEE Int. Conf. Solid-State Sens., Actuators Microsyst.*, San Francisco, CA, USA, Jan. 2005, pp. 275–278.

[109] R. D. Black, "Recent advances in translational work on implantable sensors," *IEEE Sensors J.*, vol. 11, no. 12, pp. 3171–3182, Dec. 2011.

[110] C. M. Boutry, H. Chandrahalim, P. Streit, M. Schinhammer, A. C. Hänzi, and C. Hierold, "Towards biodegradable wireless implants," *Philos. Trans. Roy. Soc. A*, vol. 370, pp. 2418–2432, Apr. 2012.

[111] E. Agu *et al.*, "The smartphone as a medical device: Assessing enablers, benefits and challenges," in *Proc. IEEE Int. Conf. Sens., Commun. Netw.*, New Orleans, LA, USA, Jun. 2013, pp. 76–80.

[112] J. M. Azzarelli, K. A. Mirica, J. B. Ravnsbæk, T. M. Swager, and M. Timothy, "Wireless gas detection with a smartphone via rf communication," *Proc. Nat. Acad. Sci.*, vol. 111, no. 51, pp. 18162–18166, 2014.

[113] R. A. Potyrailo, N. Nagraj, Z. Tang, F. J. Mondello, C. Surman, and W. Morris, "Battery-free radio frequency identification (RFID) sensors for food quality and safety," *J. Agricult. Food Chem.*, vol. 60, no. 35, pp. 8535–8543, 2012.

[114] E. Mohebi and L. Marquez, "Intelligent packaging in meat industry: An overview of existing solutions," *J. Food Sci. Technol.*, vol. 52, no. 7, pp. 3947–3964, 2015.

[115] S.-Y. Wu, C. Yang, W. Hsu, and L. Lin, "RF wireless LC tank sensors fabricated by 3D additive manufacturing," in *Proc. 18th Int. Conf. Solid-State Sens., Actuators Microsyst.*, Anchorage, AK, USA, Jun. 2015, pp. 2208–2211.

[116] A. D. DeHennis and K. D. Wise, "A wireless microsystem for the remote sensing of pressure, temperature, and relative humidity," *J. Microelectromech. Syst.*, vol. 14, no. 1, pp. 12–22, Feb. 2005.

[117] G. Asada *et al.*, "Wireless integrated network sensors: Low power systems on a chip," in *Proc. 24th Eur. Solid-State Circuits*, The Hague, The Netherlands, Sep. 1998, pp. 9–16.

[118] H. G. Schantz, "Near field propagation law & a novel fundamental limit to antenna gain versus size," in *Dig. IEEE AP-S Int. Symp.*, vol. 3A. Jul. 2005, pp. 237–240.

[119] A. M. Niknejad and R. G. Meyer, *Design, Simulation and Applications of Inductors and Transformers for Si RF ICs*. New York, NY, USA: Kluwer, 2000.

[120] P. Park, C. S. Kim, M. Y. Park, S. D. Kim, and H. K. Yu, "Variable inductance multilayer inductor with MOSFET switch control," *IEEE Electron Device Lett.*, vol. 25, no. 3, pp. 144–146, Mar. 2004.

[121] D. Golda, J. H. Lang, and M. L. Culpepper, "Two-layer electroplated microcoils with a PECVD silicon dioxide interlayer dielectric," *J. Microelectromech. Syst.*, vol. 17, no. 6, pp. 1537–1545, 2008.

[122] M. Saidani and M. A. M. Gijs, "Three-dimensional miniaturized power inductors realized in a batch-type hybrid technology," *J. Micromech. Microeng.*, vol. 12, no. 4, pp. 470–474, 2002.

[123] M. K. Kazimierczuk, G. Sancineto, G. Grand, U. Reggiani, and A. Massarini, "High-frequency small-signal model of ferrite core inductors," *IEEE Trans. Mag.*, vol. 35, no. 5, pp. 4185–4191, Sep. 1999.

[124] K. Arshak, A. Ajina, and D. Egan, "Development of screen-printed polymer thick him planner transformer using Mn-Zn ferrite as core material," *Microelectron. J.*, vol. 32, no. 2, pp. 113–116, 2001.

[125] D. Marioli, E. Sardini, M. Serpelloni, and A. Taroni, "A new measurement method for capacitance transducers in a distance compensated telemetric sensor system," *Meas. Sci. Technol.*, vol. 16, no. 8, pp. 1593–1599, 2005.

[126] G. Jacquemod, M. Nowak, E. Colinet, N. Delorme, and F. Conseil, "Novel architecture and algorithm for remote interrogation of battery-free sensors," *Sens. Actuators A, Phys.*, vol. 160, pp. 125–131, May 2010.

[127] H. S. Kim, S. Sivaramakrishnan, A. S. Sezen, and R. Rajamani, "A novel real-time capacitance estimation methodology for battery-less wireless sensor systems," *IEEE Sensors J.*, vol. 10, no. 10, pp. 1647–1657, Oct. 2010.

[128] X. Zhang and J. Chae, "Working distance comparison of inductive and electromagnetic couplings for wireless and passive underwater monitoring system of rinsing process in semiconductor facilities," *IEEE Sensors J.*, vol. 11, no. 11, pp. 2932–2939, Nov. 2011.

[129] V. Viikari, H. Seppa, and D.-W. Kim, "Intermodulation read-out principle for passive wireless sensors," *IEEE Trans. Microw. Theory Techn.*, vol. 59, no. 4, pp. 1025–1031, Apr. 2011.

[130] J. Song, V. Viikari, N. Pesonen, I. Marttila, and H. Seppä, "Optimization of wireless sensors based on intermodulation communication," *IEEE Trans. Microw. Theory Techn.*, vol. 61, no. 9, pp. 3446–3452, Sep. 2013.
[131] J. Song, J. Salmi, V. V. Viikari, and N. M. P. Pesonen, "Maximum-likelihood estimation for passive wireless intermodulation communication sensors," *IEEE Sensors J.*, vol. 14, no. 4, pp. 2280–2286, Apr. 2015.
[132] M. M. Islam, L. Rasilainen, and V. Viikari, "Implementation of sensor RFID: Carrying sensor information in the modulation frequency," *IEEE Trans. Microw. Theory Techn.*, vol. 63, no. 8, pp. 2672–2681, Aug. 2015.
[133] A. Kurs, A. Karalis, R. Moffatt, J. D. Joannopoulos, P. Fisher, and M. Soljačić, "Wireless power transfer via strongly coupled magnetic resonances," *Science*, vol. 317, no. 5834, pp. 83–86, 2007.
[134] A. P. Sample, B. H. Waters, S. T. Wisdom, and J. R. Smith, "Enabling Seamless Wireless Power Delivery in Dynamic Environments," *Proc. IEEE*, vol. 101, no. 6, pp. 1343–1358, Jun. 2013.
[135] D. A. Sanz, C. Mitrosbaras, E. A. Unigarro, and F. Segura-Quijano, "Passive resonators for wireless passive sensor readout enhancement," *Appl. Phys. Lett.*, vol. 103, no. 13, pp. 133502-1–133502-5, Sep. 2013.
[136] C. Zhang, L.-F. Wang, and Q.-A. Huang, "Extending the remote distance of LC passive wireless sensors via strongly coupled magnetic resonances," *J. Micromech. Microeng.*, vol. 24, no. 12, pp. 125021-1–125021-9, Dec. 2014.
[137] L. Dong, L.-F. Wang, C. Zhang, and Q.-A. Huang, "A cyclic scanning repeater for enhancing the remote distance of LC passive wireless sensors," *IEEE Trans. Circuits Syst. I, Reg. Papers*, to be published, doi: 10.1109/TCSI.2016.2572221.
[138] L. Dong, L.-F. Wang, and Q.-A. Huang, "A passive wireless adaptive repeater for enhancing the readout of LC passive wireless sensors," *IEEE Microw. Wireless Compon. Lett.*, vol. 26, no. 7, pp. 543–545, Jul. 2016.
[139] E. Shamonina, V. A. Kalinin, K. H. Ringhofer, and L. Solymar, "Magneto-inductive waveguide," *Electron. Lett.*, vol. 38, no. 8, pp. 371–373, Apr. 2002.
[140] S. F. Pichorim and P. J. Abatti, "A novel method to read remotely resonant passive sensors in biotelemetric systems," *IEEE Sensors J.*, vol. 8, no. 1, pp. 6–11, Jan. 2008.
[141] M. Rocznik, F. Henrici, and R. Has, "ASIC for a resonant wireless pressure-sensing system for harsh environments achieving ±2% error between –40 and 150°C using Q-based temperature compensation," in *IEEE ISSCC Dig. Tech. Papers*, Feb. 2012, pp. 202–204.
[142] S. Zhang, P. Pasupathy, and D. P. Neikirk, "Microfabricated self-resonant structure as a passive wireless dielectric constant and conductivity sensor," *Microsyst. Technol.*, vol. 18, no. 7, pp. 885–891, 2012.
[143] Q. Y. Ren, L. F. Wang, J. Q. Huang, C. Zhang, and Q. A. Huang, "Simultaneous remote sensing of temperature and humidity by LC-type passive wireless sensors," *J. Microelectromech. Syst.*, vol. 24, no. 4, pp. 1117–1123, Aug. 2015.
[144] L. Dong, L.-F. Wang, and Q.-A. Huang, "Implementation of multi-parameter monitoring by an LC-type passive wireless sensor through specific winding stacked inductors," *IEEE Internet Things J.*, vol. 2, no. 2, pp. 168–174, Apr. 2015.
[145] L. Dong, L.-F. Wang, and Q.-A. Huang, "An LC passive wireless multifunctional sensor using a relay switch," *IEEE Sensors J.*, vol. 16, no. 12, pp. 4968–4973, Jun. 2016.

Qing-An Huang (S'89–M'91–SM'95–F'16) received the B.S. degree from the Hefei University of Technology, Hefei, China, in 1983, the M.S. degree from Xidian University, Xi'an, China, in 1987, and the Ph.D. degree from Southeast University, Nanjing, China, in 1991, all in electronics engineering. His Ph.D. research was on micromachined GaAs piezoelectric sensors.

He joined as a Faculty Member with the Department of Electronic Engineering, Southeast University, where he became a Full Professor in 1996, and was appointed as the Chair Professor of the Chang-Jiang Scholar by the Ministry of Education in 2004. He is currently the Founding Director of the Key Laboratory of MEMS (Ministry of Education) with Southeast University. He has authored a book entitled *Silicon Micromachining Technology* (Science Press, 1996), and authored or co-authored four international book chapters, over 200 peer-reviewed international journals/conference papers, and holds over 100 Chinese patents.

Dr. Huang has served as the Editor-in-Chief of the *Chinese Journal of Sensors and Actuators* since 2005. He is an Editorial Board Member of the *Journal of Micromechanics and Microengineering*. He was the Conference Co-Chair of the SPIE Microfabrication and Micromachining Process Technology and Devices (Proceedings of SPIE, 2001), the TPC Co-Chair of the Sixth Asia-Pacific Conference of Transducers and Micro/Nano Technologies (APCOT) (Nanjing, 2012), and a TPC Member of TRANSDUCERS from 2009 to 2015 and the IEEE Sensors Conference from 2002 to 2015. He served as the Steering Committee Chair of APCOT from 2012 to 2014. He was a recipient of the National Outstanding Youth Science Foundation Award of China in 2003.

Lei Dong received the B.S. degree in electronics engineering from Southeast University, Nanjing, China, in 2012. She is currently pursuing the Ph.D. degree with the Key Laboratory of MEMS of the Ministry of Education, Southeast University.

Her research interests include MEMS sensors and inductors, wireless passive micro-sensor, and inductive telemetry technique.

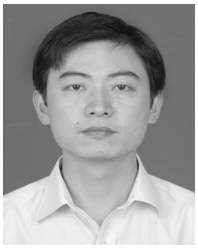

Li-Feng Wang (M'13) was born in China in 1981. He received the B.S., M.S., and Ph.D. degrees from Southeast University, Nanjing, China, in 2003, 2006, and 2013, respectively, all in electrical engineering. From 2006 to 2008, he was with the Nanjing Electronic Device Institute, where he was involved in silicon micromechanical devices.

He joined as a Faculty Member, Department of Electronic Engineering, Southeast University, as Assistant Professor. His current research interests include the design, fabrication and reliability of wireless micro-sensors, and micromachined RF/MW switches.